NAVAL AIR DEVELOPMENT CENTER

Johnsville, Warminster, Pennsylvania

REPORT NO. NADC-MA-6726 24 Jan 1968

THE EFFECTS OF HYDROSTATIC PRESSURES TO 8250 PSI ON ELECTROLYTIC HYDROGEN IN IRON

INDEPENDENT RESEARCH TASK NO. RO11-01-01
WORK UNIT NO. 33

THE EFFECTS OF HYDROSTATIC PRESSURE TO 8250 PSI ON ELECTROLYTIC HYDROGEN IN IRON

John J. DeLuccia

Naval Air Development Center
Johnsville, Pennsylvania

24 January 1968

DEPARTMENT OF THE NAVY
NAVAL AIR DEVELOPMENT CENTER
JOHNSVILLE
WARMINSTER, PA. 18974

Aero Materials Department

REPORT NO. NADC-MA-6726 24 Jan 1968

THE EFFECTS OF HYDROSTATIC PRESSURES TO 8250 PSI ON ELECTROLYTIC HYDROGEN IN IRON

INDEPENDENT RESEARCH TASK NO. RO11-01-01
WORK UNIT NO. 33

An apparatus for the determination of electrochemical parameters as well as diffusion parameters of hydrogen in iron at hydrostatic pressures up to 20,000 psi using the hydrogen permeation technique is described. Values of the diffusion coefficient and solubility of hydrogen in iron at pressures to 8250 psig are listed. The effect of pressure on the cathodic hydrogen evolution kinetics is noted. All experiments were performed on Armco iron in 0.1N H_2SO_4 + 0.001N HCl at 21°C.

Reported by: _____
J. J. DeLuccia
Chemical Metallurgy Branch

Approved by: _____
Mrs. S. J. Ketcham, Head
Chemical Metallurgy Branch

_____
F. S. Williams, Superintendent
Metallurgical Division

S U M M A R Y

INTRODUCTION

The common practice of protecting ocean going ships and other immersed structures against corrosion by the technique of cathodic protection can and most probably will be used on future undersea steel structures. Since the electrolytic production of hydrogen is a concomitant of cathodic protection, as well as many corrosion reactions, it is necessary to know the effects of deep ocean pressures on electrolytic hydrogen in iron.

This work is a progress report performed under Independent Research Task No. RO11-01-01, Work Unit No. 33, "The Electrochemical and Metallurgical Aspects of Environmental Stress Cracking of Alloys."

SUMMARY OF RESULTS

The method used in this study consisted of imposing a diffusion gradient on an iron foil by producing hydrogen cathodically on one side of the foil with the simultaneous removal of hydrogen on the opposite side via an electrochemical anodic reaction which oxidizes the hydrogen to water. The resulting current due to the hydrogen oxidation reaction is measured and this current is an instantaneous measure of the hydrogen permeation rate. The measurement of the permeation transients, at various pressures using a unique teflon timpanic cell, enabled the calculation of the diffusion coefficient and subsequent solubility calculations to be made. The inclusion of a Ag-AgCl reference electrode in the cathodic compartment enabled the hydrogen overpotential to be monitored as a function of applied pressure. The following results are for Armco iron in 0.1N H_2SO_4 + 0.001N HCl at 21°C:

(1) Applied hydrostatic pressure increases the residual hydrogen permeation rate in iron in a linear fashion to about 6000 psi. A marked increase in the permeation rate occurs between 6000 and 8000 psi.

(2) The pressure effects on hydrogen permeation are reversible within the range from 0 to 8250 psi applied pressure.

(3) Hydrostatic pressures to 6200 psi do not affect the diffusion coefficient of hydrogen in Armco iron.

(4) Solubility of hydrogen in Armco iron is proportional to the applied hydrostatic pressure at least up to 6000 psi.

(5) The partial pressure of hydrogen does not affect the hydrogen overpotential.

CONCLUSIONS

The increased solubility of hydrogen in iron at elevated pressures and low temperatures (21°C) revealed in this work necessitates an increased concern for the role of hydrogen in environmental cracking of alloys destined to be used in the deep ocean environment.

The absence of a hydrostatic pressure effect on the diffusion coefficient of hydrogen in iron indicates minimal lattice distortion and is a fact helpful in picturing the migration of H_2 in an elastic stress field.

RECOMMENDATIONS

Further work, both theoretical and experimental at various pressures, cathodic current densities, and temperatures, will be performed to explore the relatively untouched areas of pressure dependent activation energy for diffusion, diagnosis of hydrogen electrode kinetics in the linear current-overpotential region, the marked solubility increase in the 6000 to 8000 psi region, and the effect of grain size on hydrogen diffusivity in iron.

TABLE OF CONTENTS

LIST OF TABLES AND FIGURES

B A C K G R O U N D

Hydrogen atoms electrochemically produced as a result of a partial (e.g. corrosion) or total (e.g. plating or protection) cathodic reaction on the surface of iron or steel may be combined to form hydrogen gas or may enter the metallic lattice interstitially and permeate throughout the metal. The presence of hydrogen in high strength steel can cause catastrophic failure of structures in service environments. It has been shown, by Troiano, references (a) and (b), and others, that the degree of embrittlement in metals is a function of the rate of hydrogen entry into the bulk lattice from the adsorbed state.

The investigation herein described was made to determine the effects of high hydrostatic pressures found in deep ocean environments on hydrogen electrolytically produced on iron. A sensitive electrochemical method, reference (c), for determination of hydrogen permeation rates was used to determine the diffusion coefficients and permeation rates of electrolytic hydrogen through polycrystalline Armco iron. The investigation was made under carefully defined conditions of cathodic polarization, and known boundary conditions for hydrogen diffusion in a metal foil. The permeation rate, as a function of hydrostatic pressure and cathodic polarization was investigated.

1. Nature of Hydrogen Permeation Through Metals

Early work by Richardson et.al., reference (d), and later by Sieverts, reference (e), showed the solubility and also the permeability of hydrogen in metals to be proportional to the square root of the ambient hydrogen pressure, P_{H_2}, as

$$S = K\, P_{H_2}^{\frac{1}{2}} \qquad (1)$$

where S = solubility.

Thus it was concluded that hydrogen is dissolved and diffuses through metals as atoms rather than as the diatomic molecule.

Hydrogen generated electrolytically on one side of an iron foil was found to obey a relationship, reference (f), similar to Equation (1) in the form of

$$P = K\, I^{\frac{1}{2}} \qquad (2)$$

where P = permeation, I = current in electrolytic circuit.

Due to the similarity of Equation (1) and Equation (2), it was concluded that the rate controlling process was identical for diffusion studied by

vacuum methods at elevated temperatures and also electrolytically induced diffusion of hydrogen through metals.

In the studies performed by Borelius et.al., reference (f), Heath, et.al., reference (g), and Frumkin et.al., reference (h), for permeation of hydrogen through metals, the rates were determined manometrically, i.e. by measurement of the hydrogen pressure build-up at the exit side of the diffusion foil. These studies showed that for the electrolytic diffusion of hydrogen through iron, the permeation rate is inversely proportional to the thickness of the membrane and the diffusion process was the rate determining step in the overall permeation process.

2. Kinetics of Electrolytic Hydrogen Evolution and the Adsorption of Hydrogen by Metals

The surface adsorption of atomic hydrogen on the metallic substrate is important in the diffusion process. Any cathodic reaction involving the evolution of hydrogen gas need not be 100% effective. Some fraction of the evolved H_2 may permeate into the metal. It is this small fraction of evolved hydrogen which after entering the metal lattice contributes to the insidious embrittlement phenomenon in metals. Thus a knowledge of the extent of hydrogen coverage on a metal and the variation of that coverage with potential, hydrostatic pressure and temperature is of considerable importance in assessing the rate of entry of hydrogen into a metal during cathodic polarization.

The form of the Langmuir adsorption isotherm applicable to the kinetics of dissociative chemisorption is (reference (i))

$$\frac{\theta}{1-\theta} = \ell a_p \qquad (3)$$

where θ = the degree of coverage; ℓ = standard free energy of adsorption; a_p = the activity of the adsorbing gas.

In order to apply the Langmuir adsorption isotherm to the hydrogen evolution reaction on iron in aqueous acidic solutions, the following sequential reactions are assumed:

$$H_3O^+ + e^- + M \longrightarrow (M\text{-}H) + H_2O \qquad \text{Electrolytic Discharge} \qquad (4)$$

$$(M\text{-}H) + (M\text{-}H) \longrightarrow 2M + H_2\uparrow \qquad \text{Catalytic Combination} \qquad (5)$$

$$(M\text{-}H) + H_3O^+ + e^- \longrightarrow M + H_2\uparrow + H_2O \qquad \text{Electrochemical Desorption} \qquad (6)$$

Let the velocities of the forward reactions Equations (4), (5) and (6) be I_4, I_5, and I_6, respectively, and the velocities of the reverse reactions be I_{-4}, I_{-5}, and I_{-6}. If one of the above reactions is rate controlling, i.e. slowest, the fast reaction will be in equilibrium. The kinetic equations for reactions (4), (5), and (6) are as follows:

$$I_4 = FK_4\, a_{H_3O^+}(1-\theta)\ \exp\left[-\frac{\alpha F\eta}{RT}\right],\quad I_{-4} = FK_{-4}\,\theta\ \exp\left[\frac{(1-\alpha)F\eta}{RT}\right] \tag{7}$$

$$I_5 = K_5(\theta)^2\ ,\quad I_{-5} = K_{-5}(1-\theta)^2\, P_{H_2} \tag{8}$$

$$I_6 = FK_6\, a_{H_3O^+}\,\theta\ \exp\left[-\frac{\alpha F\eta}{RT}\right],\quad I_{-6} = FK_{-6}(1-\theta)\, P_{H_2}\ \exp\left[\frac{(1-\alpha)F\eta}{RT}\right] \tag{9}$$

where

I = reaction rate	η = activation overpotential $(E - E_r)$
F = Faraday constant	
θ = hydrogen coverage	T = absolute temperature
K = reaction rate constant	$a_{H_3O^+}$ = activity of hydronium ion
α = symmetry factor	
R = gas constant	P_{H_2} = H_2 gas pressure

Assume reaction (6) to be rate controlling and reaction (4) to be in equilibrium; that is, a condition of fast discharge and slow electrochemical desorption. Equating the forward and backward reaction rates of Equation (4), we have

$$K_4\, a_{H_3O^+}(1-\theta)\ \exp\left[-\frac{\alpha nF}{RT}\right] = K_{-4}\,\theta\ \exp\left[\frac{(1-\alpha)nF}{RT}\right] \tag{10}$$

$$\frac{\theta}{1-\theta} = \frac{K_4}{K_{-4}}\ a_{H_3O^+}\ \exp\left[-\frac{nF}{RT}\right] \tag{11}$$

When $\theta \ll 1$; $(1-\theta) \rightarrow 1$; so that for small θ (low hydrogen coverage) Equation (11) may be written:

$$\theta = \frac{K_4}{K_{-4}}\ a_{H_3O^+}\ \exp\left[-\frac{nF}{RT}\right] \tag{12}$$

When $\theta \cong 1$; $(1-\theta) \rightarrow 0$; so that for large θ (almost complete coverage) Equation (11) becomes

$$(1-\theta) = \frac{K_{-4}}{K_4 \, a_{H_3O^+}} \exp \frac{\eta F}{RT} \tag{13}$$

For conditions where $\theta << 1$; Equation (12) is substituted for θ in the rate equation for the controlling reaction, i.e. Equation (9), forward, to give

$$I_6 = FK_6 \frac{K_4}{K_{-4}} a^2_{H_3O^+} \exp \left[- \frac{\eta F (1+\alpha)}{RT} \right] \tag{14}$$

The relationship between the cathodic current (reaction rate 6) and the overpotential for the fast discharge-slow desorption mechanism for small hydrogen coverages ($\theta \ll 1$) is extracted from Equation (14) as

$$\frac{d\eta}{d \ln I_6} = - \frac{1}{(1+\alpha)} \frac{RT}{F} \tag{15}$$

For conditions of high coverage, $\theta = 1$, the rate controlling reaction (forward direction) becomes

$$I_6 = FK_6 \, a_{H_3O^+} \exp \left[- \frac{\alpha F \eta}{RT} \right] \tag{16}$$

Now the relationship between the current and overpotential for $\theta \cong 1$, obeying the fast discharge-slow desorption mechanism is

$$\frac{d\eta}{d \ln I_6} = - \frac{RT}{\alpha F} \tag{17}$$

Similar treatments to obtain the theoretical Tafel slopes of other possible sequential reactions were made and are given in Table 1. Table 1 also lists the permeation-cathodic current and overpotential-pressure relationships predicted for the various mechanism combinations. As an example, using the fast discharge-slow desorption mechanism with $\theta \ll 1$, the permeation-current relationships were determined by utilizing the chain

TABLE 1

HYDROGEN EVOLUTION REACTION MECHANISMS AND THEIR CORRESPONDING CURRENT-POTENTIAL-PERMEATION-PRESSURE RELATIONSHIPS

Mechanism	Tafel Slope 25°C Volts/decade $\alpha = \frac{1}{2}$	Permeation-current relation for $\alpha = \frac{1}{2}$	Overpotential Pressure Relation	θ
Fast discharge Slow desorption	0.04	$J \propto I_c^{2/3}$	$n \neq F(p)$	$\gtrsim 1$
Fast discharge Slow desorption	0.12	$J \neq f(I_c)$	$n \neq f(p)$	$\gtrsim 1$
Fast desorption Slow discharge	0.04	$J \neq f(I_c)$	$n = f(p)$	$\gtrsim 1$
Fast discharge Slow combination	0.03	$J \propto I_c^{1/2}$	$n \neq f(p)$	$\ll 1$
Fast combination	0.12	$J \neq f(I_c)$	$n \neq f(p)$	$\ll 1$
Slow discharge	0.12	$J \neq f(I_c)$	$n = f(p)$	≈ 1
Coupled discharge and combination	0.12	$J \propto I_c^{1/2}$	$n \neq f(p)$	1
Coupled discharge and desorption	0.12	$J \neq f(I_c)$	$n \neq f(p)$	1

rule on partial derivatives of Equation (11) and Equation (14), i.e.

$$\frac{\partial \ln \theta}{\partial \ln I} = \frac{\partial \ln \theta}{\partial \eta} \cdot \frac{\partial \eta}{\partial \ln I} \tag{18}$$

$$\frac{\partial \ln \theta}{\partial \ln I} = \frac{F}{RT} \left(\frac{1}{1+\alpha}\right) \frac{RT}{F} \tag{19}$$

for $\alpha = \frac{1}{2}$

$$\frac{\partial \ln \theta}{\partial \ln I} = \frac{1}{1+\alpha} = \frac{2}{3} \tag{20}$$

so that

$$\theta \propto I^{2/3} \tag{21}$$

If the assumption of proportionality between permeation and hydrogen surface coverage is made, we may write,

$$J \propto I^{2/3} \tag{22}$$

Thus, an analysis of the electrode kinetics of various consecutive steps in the hydrogen evolution reaction gives Tafel slopes, which, in some cases, can be characteristic of the mechanism and coverage conditions. For example, if the overvoltage-current density plot exhibits a break in Tafel behavior, i.e. different slopes, Table 1 can be invoked as a diagnostic criterion to determine the change in reaction mechanism.

3. The Mathematics of Hydrogen Diffusion Through Iron

It is generally believed that hydrogen diffuses through iron atomically via an interstitial mechanism. Consider the diffusion experiment represented by the following conditions: a metallic foil of thickness L, a concentration gradient represented by C_0 on one side of the membrane; i.e., at $x = 0$ and C_L on the other side, i.e. at $x = L$. At $x = 0$, the hydrogen concentration is finite and at $x = L$, $C_L = 0$. In the present work, these boundary conditions were maintained electrochemically. The overall problem may be represented by Fick's second law for constant D as

$$\frac{\partial^2 C}{\partial x^2} - \frac{1}{D}\frac{\partial C}{\partial t} = 0 \qquad (23)$$

where D = diffusion coefficient, c = concentration, t = time.

The initial and boundary conditions pertaining to the experiment are:

$$C = C_0 \; ; \quad x = 0 \; ; \quad t \geqslant 0 \qquad (24)$$

$$C = 0 \; ; \quad x = L \; ; \quad t \gtrless 0 \qquad (25)$$

$$C = 0 \; ; \quad 0 < x < L \; ; \quad t < 0 \qquad (26)$$

The method of solution to Equation (23) reproduced here is according to McBreen, et.al., reference (j), and the numerous typographical errors of that study have been corrected.

The utilization of Fick's first law

$$J = -D\frac{\partial c}{\partial x} \qquad (27)$$

where J = steady state flux of hydrogen, and an operational solution to Equation (23) are used to define the hydrogen concentration contour within the thickness of the metal. The operational method of Laplace transformation of Equation (23) and the boundary conditions Equation (24) and Equation (25) yields

$$\frac{d^2\overline{C}}{dx^2} - \frac{p}{D}\overline{C} = 0 \qquad (28)$$

$$\overline{C} = \frac{C_0}{p} \; ; \quad x = 0 \qquad (29)$$

$$\overline{C} = 0 \; ; \quad x = L \qquad (30)$$

where $\bar{C} = L\{C(x,t)\}$, the Laplace transform operator; p = the Laplace transform parameter. A homogeneous solution for Equation (28) is

$$\bar{C} = a \exp\left[-qx\right] + b \exp\left[+qx\right] \tag{31}$$

where a and b are undetermined coefficients and $q = \left(\frac{p}{d}\right)^{1/2}$. Solving for a and b by use of Equation (29) and Equation (30) and performing the operation of inverse transformation gives

$$\frac{C(x,T)}{C_0} = \sum_{n=0}^{\infty} (-1)^n \operatorname{erfc} \frac{x + 2nL}{2\sqrt{Dt}} - \sum_{n=0}^{\infty} (-1)^n \operatorname{erfc} \frac{2L(n+1)-x}{2\sqrt{Dt}} \tag{32}$$

where $C(x,t)$ is the hydrogen concentration at x at any time t. The flux J of Equation (27) transformed to electrochemical terms is

$$J = \frac{J_t}{ZF} \tag{33}$$

where J_t is the permeation current at any time t; Z = number of electrons involved in the hydrogen oxidation reaction, and F = Faraday, 96,500 coul./eq. Fick's first law may now be written as

$$J_\infty = \frac{D_Z F}{L} (C_0 - C_L) \tag{34}$$

where J_∞ = steady state permeation current. The permeation current at any time t will be given by

$$J_t = -D_Z F \left(\frac{\partial C_{(t)}}{\partial x}\right)_{x=L} \tag{35}$$

Noting that $C_L = 0$ in Equation (34) and differentiating Equation (32) with respect to x for insertion into Equation (35) produces the relationship for fractional attainments of the steady state permeation current, i.e.

$$\frac{J_t}{J_\infty} = \frac{2}{\pi^{1/2}} \frac{L}{(Dt)^{1/2}} \sum_{n=0}^{\infty} (-1)^n \exp\left[-\frac{L(2N+1)^2}{4Dt}\right] \tag{36}$$

The first term in Equation (36) gives results valid up to 96.5% attainment of the steady state permeation, i.e.,

$$\frac{J_t}{J_\infty} = \frac{2}{\pi^{1/2}} \frac{1}{\tau^{1/2}} \exp\left[-\frac{1}{4\tau}\right]; \quad 0 < \tau < 0.5 \tag{37}$$

where $\tau = \frac{Dt}{L^2}$, a dimensionless parameter. Table 2 gives values of J_t/J_∞ for various τ.

Using Equation (37), it is possible to calculate the diffusion coefficient of hydrogen in the metal by finding the time required to attain any fraction of the steady state permeation. From Table 2, it is seen that $\tau = 0.25$ corresponds to a fractional attainment of 0.8303; thus the time it takes for J_t to reach 83% of J_∞ would be used to calculate the diffusion coefficient, i.e.,

$$D = \frac{0.25\ (L)}{t_{0.83}} \tag{38}$$

It is, therefore, possible to calculate D for any value of time t during the transient.

A corresponding Fourier solution of Equation (23) with boundary conditions given by Equations (24), (25), and (26) according to Devanathan and Stachurski, reference (c), yields:

$$\frac{J_t}{J_\infty} = 1 + 2 \sum_{n=0}^{\infty} \cos n\pi \exp\left[-Dn^2\pi^2\ t/L^2\right] \tag{39}$$

The comparable one-term solution using this method gives

$$\frac{J_t}{J_\infty} = 1 - 2 \exp\left[-\pi^2\tau\right] \tag{40}$$

This solution is valid for long times (i.e., when J_t approaches J_∞). Values of J_t/J_∞ based on this equation are also given in Table 2. Both functions are plotted against τ in Figure 1. For the region $\tau < 0.14$, the Fourier solution is invalid; there is good agreement between the two solutions in the range $0.14 < \tau < 0.3$. For $\tau > 0.3$, the Fourier solution is valid. From these two solutions, it is evident that the Laplace transform method gives a solution which can be used in its simplified first term form to give short time diffusion behavior.

TABLE 2

FRACTIONAL ATTAINMENTS OF THE STEADY STATE AS CALCULATED FROM THE FIRST TERM LAPLACE TRANSFORM AND FOURIER SERIES SOLUTIONS

τ	$\frac{2}{\pi^{1/2}} \frac{1}{\tau^{1/2}} \exp[-1/4\tau]$	$1 - 2 \exp[-\pi^2\tau]$
0.00	0.0000	-1.0
0.01	0.0000	-0.8122
0.02	0.0000	-0.6481
0.05	0.0339	-0.2210
0.10	0.2924	+0.2548
0.15	0.5500	0.5450
0.20	0.7227	0.7222
0.25	0.8303	0.8304
0.30	0.8955	0.8966
0.40	0.9470	0.9614
0.50	0.9677	0.9856
0.60	0.9596	0.9946
0.70	0.9435	0.9980
0.80	0.9178	0.9992
0.90	0.8962	0.9997
1.00	0.8788	0.9998

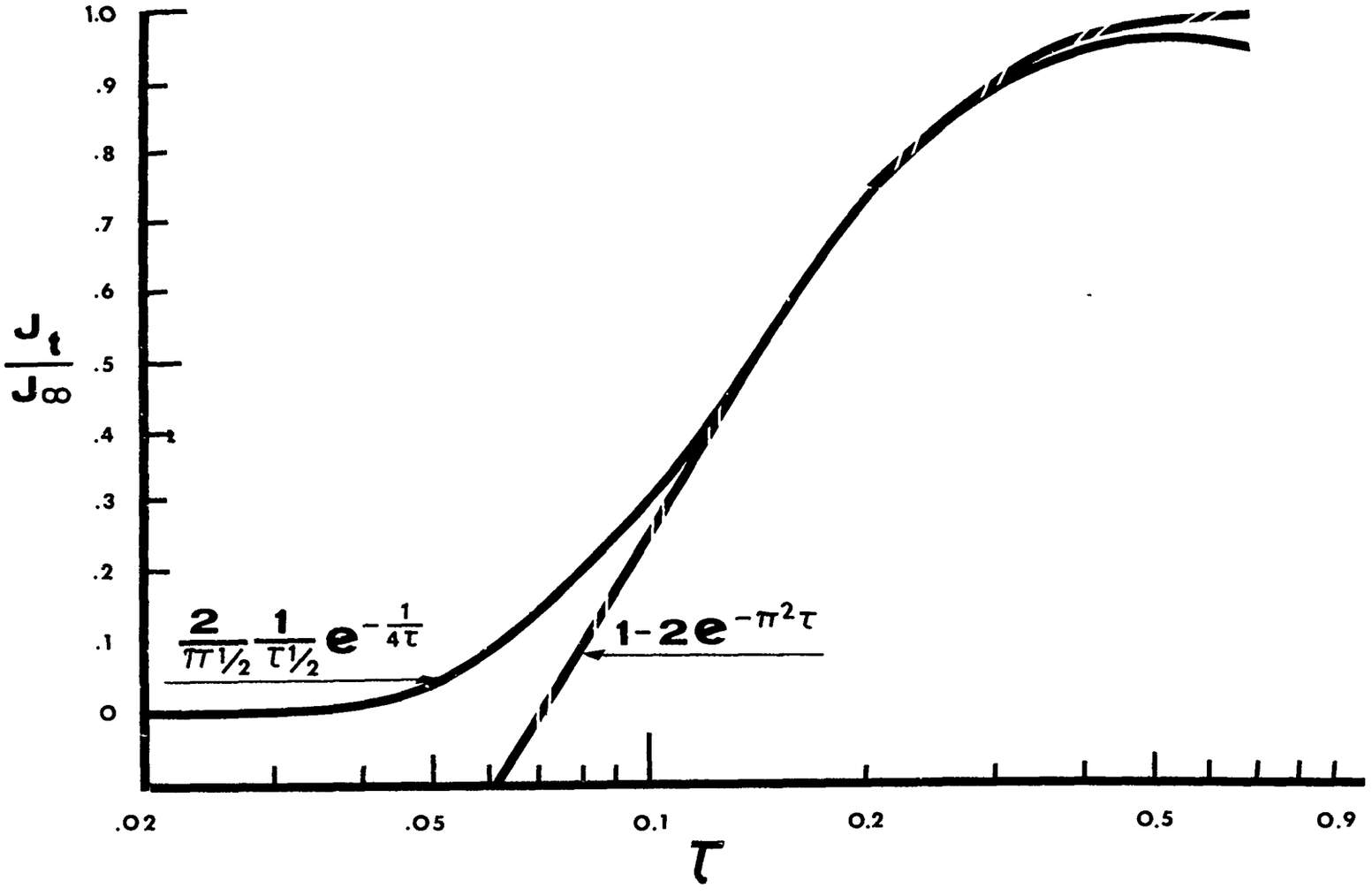

FIG. 1 COMPARISON OF THE FIRST TERM SOLUTION TO FICK'S SECOND LAW

NADC-MA-6726

E X P E R I M E N T A L

1. Requirements of Experimental Method for Investigation of Electrolytic Hydrogen Permeation Through Metal Foils Under Hydrostatic Pressure

The investigation required the electrometric measurement of the permeation rate of hydrogen through polycrystalline foils of Armco iron while under hydrostatic pressure and at constant temperature. It was essential to use a method of measurement by which the permeation rate could be continuously monitored, the diffusion coefficient of hydrogen in the metal determined, and the concentration profile of hydrogen in the metal evaluated. Since the permeation rate of hydrogen through metallic foils is relatively small, a sensitive method of detection of diffused hydrogen adapted to withstand hydrostatic pressures was necessary.

2. Principle and Description of Method

The method used in this study consisted of imposing a diffusion gradient on the metal foil by producing hydrogen cathodically on one side of the foil with the simultaneous removal of hydrogen on the opposite side. Continuous removal of hydrogen is accomplished by an electrochemical anodic reaction which oxidizes the hydrogen to water. The method was developed by Devanathan et.al., reference (c), with further refinements of the technique and mathematics made by McBreen and Nanis, reference (j).

The diffusion, or anodic, side of the foil is kept at a constant electrochemical potential, via an electronic potentiostat, that is sufficiently anodic so as to oxidize to water all of the hydrogen which arrives at the diffusion side. The resulting current due to the hydrogen oxidation reaction is measured and this current J, is an instantaneous measure of the hydrogen permeation rate, i.e.

$$\frac{J}{ZF} = -D\left(\frac{dC}{dx}\right)_{x = L} \qquad (35)$$

where Z = no. of electrons involved in the reaction
F = Faraday 96,500 coul./eq.
D = diffusion coefficient of hydrogen in iron, $cm^2\ sec^{-1}$
C = concentration of hydrogen, moles/cc Fe.
x = distance from cathodic interface, cm.
L = thickness of membrane, cm.

With this method, it is possible to continuously monitor the hydrogen permeation rate by recording the oxidation current transient that occurs during cathodic charging.

The potentiostating of the diffusion side of the membrane yields the requirement of zero hydrogen concentration directly beneath the diffusion (anodic) surface of the membrane. This fixed zero concentration boundary condition facilitates the solution of the pertinent diffusion equations (viz. Equation (23) and Equation (27)) and allows the evaluation of the hydrogen concentration profile in the iron at any instant after the initiation of cathodic charging on the input side.

Since the permeation cell was expected to function at hydrostatic pressures of up to 15,000 psi, radically new designs, materials and techniques were developed so that sensitive electrochemical measurements could be made fulfilling the important requirements of system purity and leak tightness of the cell and the electrochemical measuring components; i.e. counter and reference electrodes. The arrangement is shown diagrammatically in Figure 2.

3. Apparatus

a. The Permeation Cell and Specimen Holder

The electrochemical cell used is shown diagrammatically in Figure 3.

The drum head or timpanic principle was used to transfer pressure from the water surrounding the cell to the electrolytes in the identical timpanic cell compartments; (A) cathodic and (C) anodic c.f. Figure 3. The cell compartments were made of machined Teflon as were the threaded portions of the reference Ag-AgCl electrodes (E) and platinized platinum counter electrodes (F). The timpanic membranes (H) consisted of 0.003 inch thick Kel-F which is a strong, resilient and inert fluorinated hydrocarbon. A pressure-proof seal between the timpanic membrane and the cell compartment was achieved by pressure on a phenolic hold-down ring (K) transmitted through the double "O" rings (J) by the threaded plexiglas end caps (I). A pyrex glass Luggin capillary (L) was fitted to the Teflon extensions on each reference electrode. The cell ports accommodating the electrodes and filling plugs were all externally sealed via neoprene "O" rings (M). The electrical leads from each electrode (stranded copper wire sheathed in polyethylene and neoprene) terminated in high pressure female connectors which fit onto male connectors specially insulated from the monel pressure vessel head (c.f. Figure 2 (D)). These electrical connectors are products of the Joy Manufacturing Company and can withstand 20,000 psi working hydrostatic pressure.

The specimen holder, (B) Figure 3, serves the dual function of exposing a constant foil area of 1.27 cm^2 to the anodic and cathodic solutions and providing electrical continuity from the specimen to the monel head connector via a female-to-female Joy connector (c.f. Figure 3 (G)).

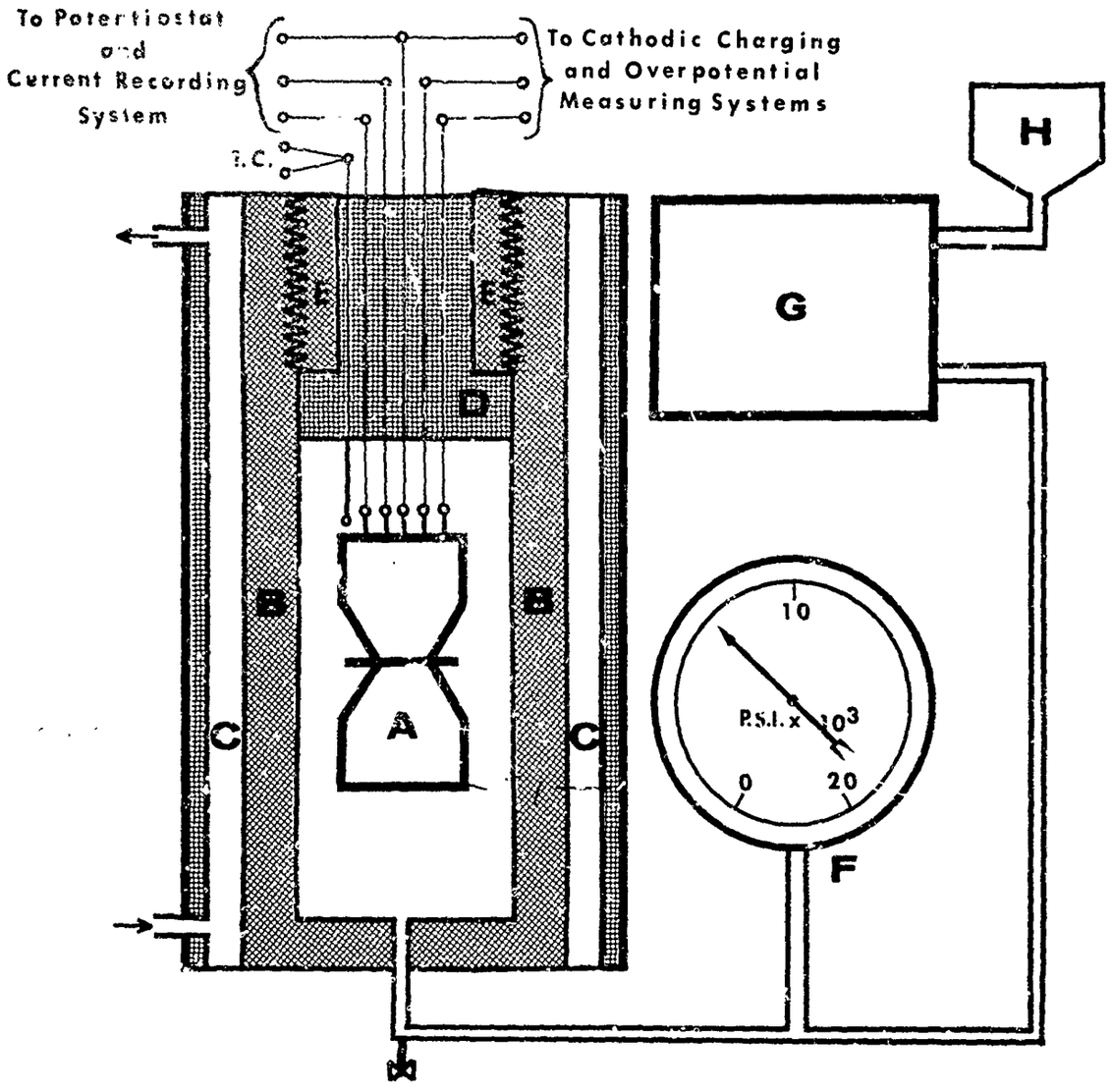

FIG.2 SCHEMATIC REPRESENTATION OF THE EXPERIMENT

LEGEND TO FIGURE 2

A. Permeation Cell

B. Pressure Vessel

C. Temperature Controlled Water Jacket

D. Monel Pressure Vessel Head

E. Retaining Ring

F. High Pressure Bourdon Type Gauge

G. Double Action, Air-actuated Hydrostatic Pressure Pump

H. Pressurizing Water Reservoir

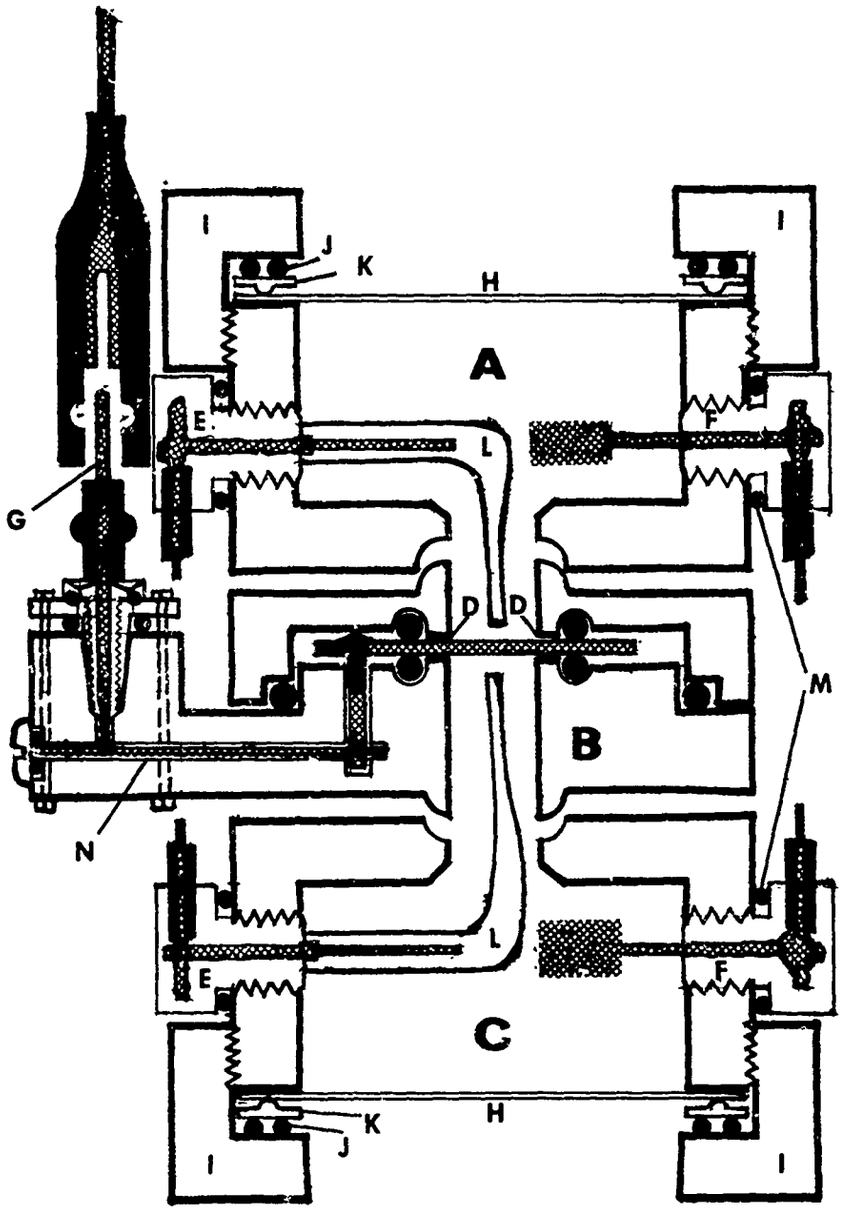

FIG.3 CROSS SECTION OF THE PERMEATION CELL

The specimen holder was machined from Teflon and is shown in Figure 3. All exposed portions are sealed via neoprene "O" rings. The Teflon extensions at the specimen-electrolyte interfaces (D) serve as gaskets, sealing out the electrolyte from the unexposed portion of the specimen. A neoprene "O" ring backs up the Teflon ring to insure sealing. The electrical connection of the specimen is made through an .08" diam. machine screw holding the specimen tc a vertical brass post. The horizontal brass rod, fitted with a plastic machine screw accommodating an "O" ring, is tapped to screw into the drilled and tapped vertical post. The final connection is made by a spring-loaded male Joy connector onto the horizontal brass rod. The cross-hatched areas of (N) and (G) in Figure 3 depict the aforementioned connections.

Timpanic compartments (A) and (C) are fitted and sealed onto the specimen holder (B) via the annular protrusions of (B) into the annular trenches of (A) and (C) and are held together by four stainless steel tie bolts through holes in the plexiglas end caps (not shown in Figure 3).

The timpanic permeation cell thus described fulfills the important requirement of purity since all internally wetted portions consist of Teflon, Kel-F or Pyrex glass, all of which contribute minimally to solution contamination.

b. Reference Electrodes

Most electrochemical studies utilize the standard reference electrodes of either the hydrogen or calomel types. Since this study requires a pressure insensitive reference electrode, the aforementioned standard electrodes could not be used. The relatively stable, solid Ag-AgCl electrode was chosen as the reference for this work.

Solid high purity silver wires .160 cm. in diam., 5 cm. in length were torch brazed to the ends of the standard copper wires of female Joy connectors. The wires were to be inserted into machined and treated Teflon shells (c.f. Figure 3 (E)). The interior hollow of each Teflon shell, about 3 cc in volume, was treated with Tetra-Etch, a special compound to etch the surface so that subsequent encapsulating materials would form a bond with the Teflon. The commercially available treating compound contained metallic sodium which when placed on Teflon, reacted to remove fluorine surface atoms and thus promote bonding. The silver wires brazed to the connectors were positioned within the Teflon electrode shells so that 2.7 cm. of silver protruded from each Teflon end. The silver wires were then encapsulated in the Teflon shells with a 2 part epoxy encapsulant specially formulated for ductility. (80% Ciba Araldite 6010; 20% Ciba Araldite 508, for ductility; N-Amino-ethylpiperazine hardener) The epoxied assembly was cured at 150°F for 2 hours. The exposed silver wires of the encapsulated electrodes were then "chloridized" to yield a thin layer of plum colored AgCl on the surface.

Chloridizing the silver wires to Ag-AgCl electrodes consisted of the following:

(1) Silver surface lightly abraded to a "4/0" paper finish
(2) Degreased in ethyl alcohol and acetone
(3) Chloridized (reference (k)) as an anode at a current density of 40 mA/cm^2 for 40 minutes in 0.1N HCl
(4) Thoroughly rinsed in distilled water

The new Ag-AgCl electrodes were aged for 1 day in distilled water to remove excess chloride ion then placed in 0.2 NaOH + 0.01N NaCl aqueous solution for potential monitoring. The NaOH solution is used as the anodic compartment electrolyte. The NaCl was added so that an equilibrium would be maintained between the AgCl and Cl^-. The electrodes stabilized to within ±0.5 mv of each other after five days in the test solution. The electrodes were then stored in distilled water for future use. These electrodes have a reversible potential of +0.240 volts with respect to the normal hydrogen electrode in aqueous solutions containing 10^{-2} moles Cl^-. For the solution in the cathodic compartment, 0.1N H_2SO_4 + 0.001N HCl, the Ag-AgCl electrodes have a reversible potential of +0.399 volts with respect to the normal hydrogen electrode.

Eight encapsulated Ag-AgCl electrodes were monitored for potential deviations as a function of pressure in both the anodic and cathodic electrolytes. Using one of the electrodes as a reference, the potentials of the other electrodes were measured and recorded with a digital voltmeter and printer. After 2 days at ambient pressure, there was a maximum of 1 mv deviation in the seven electrodes so tested. Pressurizing to 6000, 12,000 and 18,000 psi for two day periods produced no change in potential between the electrodes. Repeated pressurizing and de-pressurizing had no noticeable effect on the potential.

c. Platinum Counter Electrodes

Platinized platinum electrodes served as counter electrodes in each timpanic compartment (c.f. Figure 3 (F)). The encapsulation process for the platinum wires was identical to that used for the silver wires described in b. above. A rectangular piece of platinum wire gauze (270 mesh), 2 cm. by 1 cm. was torch fusion welded to the wire so as to make a flag. The platinum gauze was then concentrically rolled (as a flag would be furled) to a cylindrical diameter of about 3/16 inches. Each electrode was platinized in a 3% chloro-platinic acid solution containing 0.02% lead acetate at a current density of 80 mA/cm^2 alternating the polarity every 5 minutes for a period of 30 minutes. The particles of finely divided platinum on the platinum gauze surface yielded an extremely large active surface area, a prerequisite for counter electrodes.

d. Environmental Simulation Unit

Conditions necessary to achieve simulated deep ocean pressures with controlled temperatures were obtained using the environmental simulation unit shown in Figure 2 (c.f. (B) through (H)).

The pressure vessel (Figure 2 (B)) consists of a basic 2 inch thick, high-toughness cylindrical steel shell. The inner cylindrical portion of the steel vessel is pressure clad with monel metal for corrosion resistance. The internal dimensions of the pressure chamber are 5" in dia. by 19" in length. A concentric steel jacket that houses circulated cooling water (C) surrounds the outer portion of the vessel. The temperature within the vessel was pre-set and noted via an iron-constantan thermocouple (c.f. Figure 2) and a potentiometer (not shown). The temperature within the vessel was controlled to ±1°C via circulation of coolant from a combination refrigeration-heating unit not shown in Figure 2.

Suitable access to the pressure chamber to monitor electrochemical changes with the permeation cell (c.f. Figure 2 (A)) was provided via eight electrode ports through the monel head (c.f. Figure 2 (D)). The electrical connectors through each port consist of a 1/8" dia. stainless steel rod silver brazed to the end of the center post adjacent to the threaded portion of a male Joy connector and encased in a Kel-F tube to prevent short circuiting with the monel head. The male Joy connectors were then screw-sealed into the monel head. Since the metallic center post of each male Joy connector is insulated from the threaded portion, (c.f. Figure 3 (G)) a completely insulated and pressure sealed electrical path was achieved from each electrode connection in the permeation cell through the monel head and to the external electrical systems. When finally positioned, the monel head was secured by a 6" deep, threaded steel retaining ring (c.f. Figure 2 (E)).

The hydrostatic pressures necessary for the experiment were achieved by pumping water into the constant volume pressure chamber containing the timpanic permeation cell. A double-action, air-operated pump (c.f. Figure 2 (G)) supplied with distilled water as a pressurizing fluid from the reservoir (H), forced water into the pressure chamber through high pressure (40,000 psi bursting strength) monel tubing to achieve pressures to 10,000 psi within a period of 30 seconds. Pressures within the chamber were read directly on a Bourdon tube type Heise pressure gage on the line (c.f. Figure 2 (F)). Pressure control was maintained by a pressure valve from the line (90 lbs.) to the pump and a drain valve shown at the bottom of the vessel (Figure 2).

e. Electrical Circuit

The cathodic or charging compartment was provided with a constant cathodic current by a Harrison D.C. power supply (E) output 0 - 40V;

0 - 400 mA. (c.f. Figure 4). The current from this supply was passed through a variable resistor, R , adjusted to give required currents read on the ammeter I_c. The potential of the iron foil cathode surface was measured against an Ag-AgCl reference electrode using a high impedance (10 meg ohm) Beckman digital voltmeter and recorded by a Beckman digital printer.

Polarization on the anodic side of the foil was effected by use of an Anotrol, model 4700, electronic potentiostat (c.f. Figure 4). A constant potential was maintained on the foil surface by the potentiostat. The current delivered by the potentiostat to keep the anodic potential constant was monitored by allowing it to cross a 10-ohm precision resistor (c.f. Figure 4). The resulting voltage was fed into a Keithley electrometer acting as an amplifier (10 mv output for full scale deflection) and this output was in turn fed to a Moseley 680 strip chart recorder which recorded the signal as the permeation or anodic current (c.f. Figure 4 (I_a)). The Moseley recorder had a full scale sweep time of one-half second so that good precision was possible in recording current time transients.

4. Preparation of Materials

a. Preparation of Iron Specimens

One inch wide strips of hot rolled 1 mm. thick Armco iron were obtained from the Electrochemistry Laboratory of the University of Pennsylvania. Specimens 2.54 cm. long were cut using an abrasive cut off wheel. A countersunk hole was drilled at one corner of each specimen to accommodate an .080" machine screw used to secure the specimen to the electrical contact system of the specimen holder (c.f. Figure 3). The specimens were then annealed at 900°F for 1 hour to remove residual stresses. Each side of the specimens or foils was prepared by metallographic dry polishing, to "4/0" abrasive paper. The foils were then annealed a second time in an Argon atmosphere (900°F for ½ hour) to remove any residual stresses of processing. At this point, the specimens measured 0.96 mm. in thickness, and had an A.S.T.M. grain size number of 7.

The following surface preparation, reference (1), which was found to give reproducible results in electrochemical testing, was used on the foil specimens:

(1) degreased in benzene; wiped dry with cotton;

(2) immersed and swabbed in 2% HCl/methyl alcohol solution for 1 minute at room temperature; rinsed in methyl alcohol, cold air dried;

(3) immersed and swabbed in 2% H_2SO_4/methyl alcohol solution for 3 minutes at room temperature; rinsed in methyl alcohol, hot air dried to remove solution; cooled to room temperature.

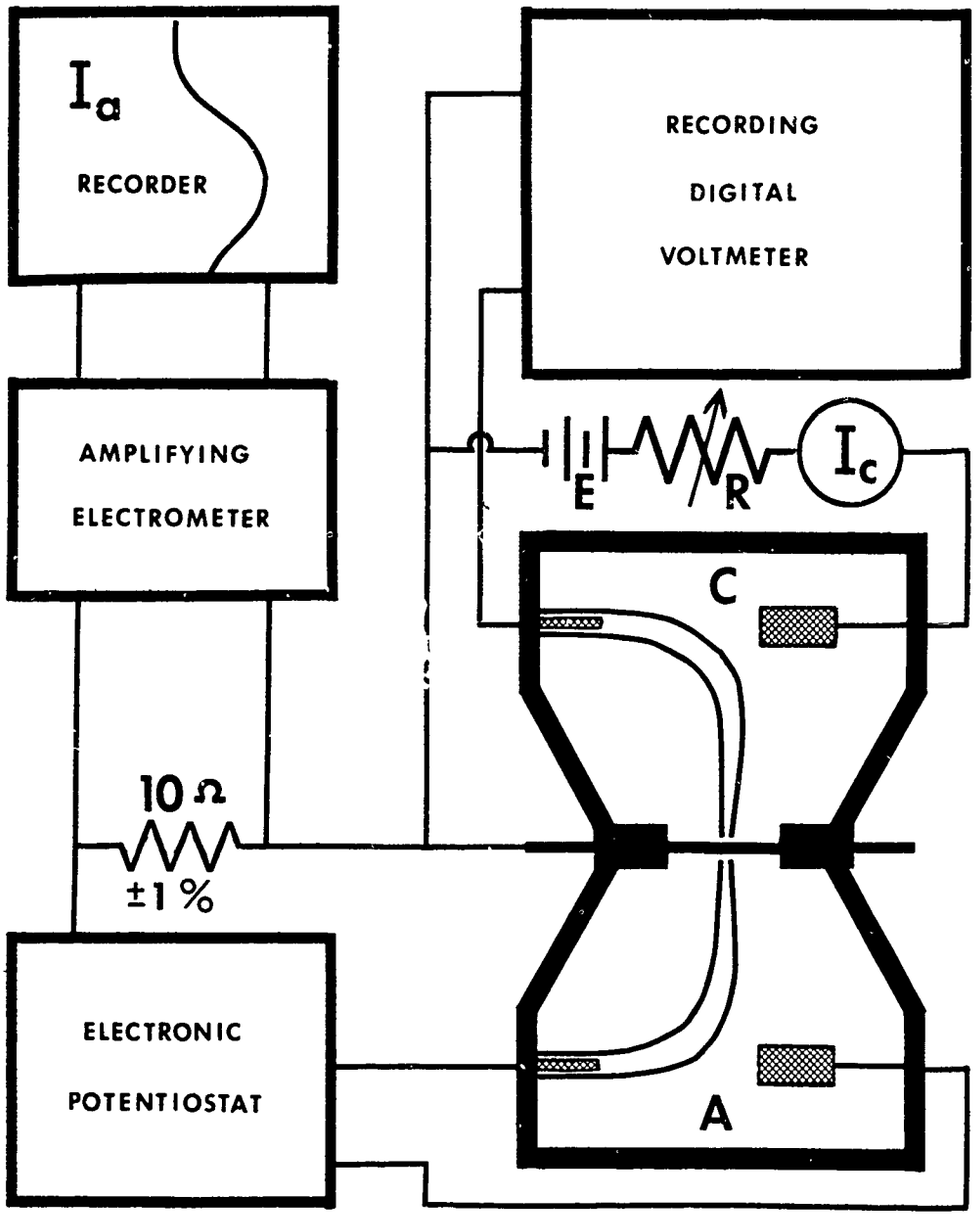

FIG. 4 THE CIRCUIT DIAGRAM

The side on each foil opposite the countersunk was chosen as the side to be exposed to the anodic compartment and hence the side to be plated with palladium. The inert palladium coating on iron is necessary in the anodic compartment since the imposed anodic polarization would cause severe corrosion of an unprotected surface and would result in changing boundary conditions. Palladium is exclusively used in this regard since it resists corrosion; and the diffusivity of hydrogen though it is extremely high and hence will not be a barrier to diffusing hydrogen atoms at the iron-palladium interface. An electroless palladium plating technique was used immediately after step three of the surface preparation. The application of approximately 1 ml. of "Pallamerse" solution in a circular motion over a 2 cm. dia. area caused a good Pd coating of $\approx 10^{-6}$ cm. thickness after one hour of exposure. The excess solution was removed by thorough rinsing with distilled water followed by acetone rinsing to remove the water. The specimens were then wrapped in soft tissue paper and stored in a dessicator.

b. Preparation of Test Solutions

The 0.2N NaOH + 0.01N NaCl solution used in the anodic compartment was prepared by dissolving Baker analyzed reagent (electrolytic pellets) of sodium hydroxide and sodium chloride in doubly distilled water having a conductivity of 1 million ohms measured with a conductivity bridge having a cell constant of 0.1. The choice of 0.1N H_2SO_4 + .001N HCl as the solution in the charging or cathodic compartment was made only after it was experimentally determined to cause little corrosion on Armco iron (0.5 mg dm^{-2} day^{-1}) when totally de-aerated. The sulfuric and hydrochloric acids were Baker analyzed reagent grade.

5. Procedure for Pressure-Permeation Run

a. Before Run

All solid Teflon and Kel-F parts of the permeation cell were cleaned in boiling concentrated reagent grade nitric acid for ½ hour, thoroughly rinsed in distilled water and stored in conductivity water until used. All other parts of the cell such as neoprene "O" rings, not internally wetted, were cleaned with a laboratory alkaline cleaner and stored in distilled water.

The electrolyte solutions were freshly prepared 24 hours before a scheduled run and were de-aerated prior to use by diffusing ultra-pure helium (99.99%) gas through one liter of each solution at a rate of 10 cu.ft./hr. for 16 hours. It is important to eliminate oxygen in both the cathodic and the anodic compartments. In the cathodic compartment, oxygen will act as a depolarizer and stimulate corrosion of the iron surface in the absence of a cathodic current. In the anodic compartment, the presence of oxygen will cause some of the imposed current to be used in its reduction rather than for its intended purpose, namely to oxidize diffused hydrogen atoms.

In order to avoid contamination during handling, vinyl gloves were used to manipulate all parts of the permeation cell during its assembly. The Luggin capillaries were filled with appropriate electrolyte and fitted to the Teflon protrusions on each of two Ag-AgCl reference electrodes. The reference and counter electrodes were then tightly screwed into the walls of the timpanic compartments causing the "O" rings (c.f. Figure 3 (M)) to effect a seal. The iron foil was then secured, palladium surface facing down, in the specimen holder with a 0.080" dia. stainless steel machine screw (c.f. Figure 3) and the top portion of the holder secured to the bottom portion by nine machine bolts (now shown) equally distributed along the outer circumference. Thus, the three neoprene "O" rings at the central portion of (B) and the Teflon gaskets at (D) were compressed to provide a seal. Timpanic compartments (A) and (C) were sealed to specimen holder (B) by four stainless steel tie bolts (not shown) spanning the two plexiglas end caps. The assembled permeation cell was then filled with appropriate electrolyte under Helium gas pressure; the filling port quickly sealed, and the cell attached to the monel head suspended above the pressure vessel. The cathodic compartment was assigned the uppermost position as shown in Figure 3, region (A), since any accumulation of gaseous hydrogen would occur at the timpanic membrane and not at the foil surface to interfere with the hydrogen reaction. Appropriate electrical connections to the head were made and the cell was then lowered into the pressure vessel. The retaining ring was finally secured and appropriate external electrical connections made so that a run was possible.

b. The Pressure-Permeation Run

Before a permeation run was made, all of the residual hydrogen that was in the iron foil was removed and oxidized on the anodic side by potentiostating the specimen prior to charging with hydrogen via a controlled cathodic current on the input or cathodic side. The specimen was potentiostated at -315 mv. (vs. Ag-AgCl) (-75 mv. vs. N.H.E.) and the resulting residual permeation current was recorded. When the residual anodic current reached a steady state ($<10^{-6}$ A/cm^2), hydrogen was generated on the opposite side by activating the circuit in the cathodic compartment. The instant in time of initiation of cathodic polarization was noted on the chart for recording the permeation transient, and the permeation was measured simultaneously with the cathodic (charging) current and cathodic potential. The instant of cathodic current input was marked by a jump in permeation current prior to hydrogen breakthrough time. This jump is caused by a terminal resistance within the circuit on the order of milliohms. This effect was neglected in plotting the transient.

The initial runs were at ambient (atmospheric) pressure with successive runs performed at higher pressures. Two final runs were performed at ambient pressure after the pressure-permeation runs to verify the observed effects. The cathodic current was interrupted after each run so that successive runs established new residual permeation currents independent of any imposed cathodic charging.

R E S U L T S

All permeation results are for polycrystalline Armco iron foil (0.96 mm. thick) in 0.1N H_2SO_4 + 0.001N HCl solution at 21 ± 1°C.

1. Effect of Hydrostatic Pressure on Residual Hydrogen Permeation

The residual permeation current (no cathodic charging) as a function of the applied hydrostatic pressure is shown in Figure 5. This effect is reversible, i.e. on releasing the pressure, the residual permeation current returns to its original value ($< 10^{-6}$ A/cm^2). The time to reach a steady state residual current for successive pressures was always approximately 12 seconds up to the 6200 psi value. The time to reach a steady state current following the pressure step from 6200 psi to 8250 psi was 19 minutes.

2. Effect of Pressure on the Diffusion Coefficient and the Measured Solubility of Hydrogen in Armco Iron

The mathematics of the method used to determine D from permeation transient data has been described in Background, paragraph 3. If the diffusion process actually conforms to the chosen boundary conditions, a plot of J_t/J_∞ (experimental) versus log t and of $\frac{2}{\pi^{1/2}} \frac{1}{\tau^{1/2}}$ $\exp\left[-1/4\tau\right]$ against $\log \tau$, should have the same shape and the difference in the abscissa should be a constant; i.e. log D/L^2. Fractional current attainment plots vs. log t for permeation transients at various pressures and cathodic current densities exhibited good shape agreement with the first term Laplace transform solution (c.f. Figures 6 and 7). This indicates that the initial and boundary conditions for diffusion have been correctly chosen, i.e. the steady state concentration C_0 is set up instantaneously at the input surface; the steady state hydrogen concentration at the anodic (consumption) surface is constant since the diffusion coefficient is constant. The calculations of D and the solubility of hydrogen (concentration of hydrogen at the input surface) as a function of pressure are shown in Table 3. The concentrations were evaluated according to Equation (34) using the steady state residual permeation current for J_∞ noted at the particular pressure and the calculated value of D. The calculated concentrations as a function of the applied pressure are shown in Figure 8. The concentrations for data points at 600 psi and 2700 psi noted in Figure 8 but not appearing in Table 3, were calculated using a $D = 4.3 \times 10^{-5}$ cm^{2}sec^{-1} since it was noted that D is independent of pressure. Figure 9 is a plot of hydrogen concentration as a function of the square root of the applied pressure.

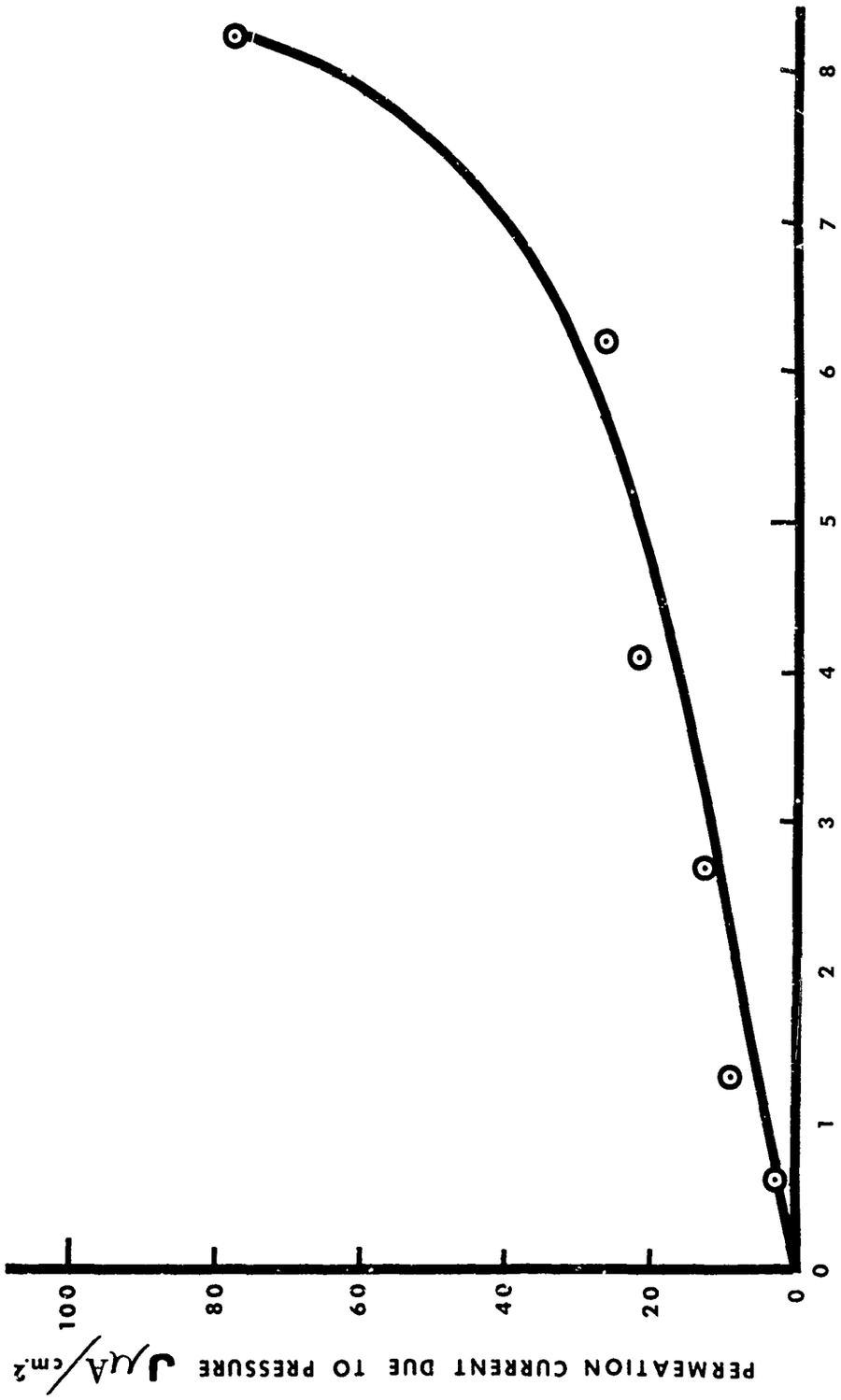

FIG. 5 RESIDUAL PERMEATION CURRENT VS. APPLIED HYDROSTATIC PRESSURE AT 21°C

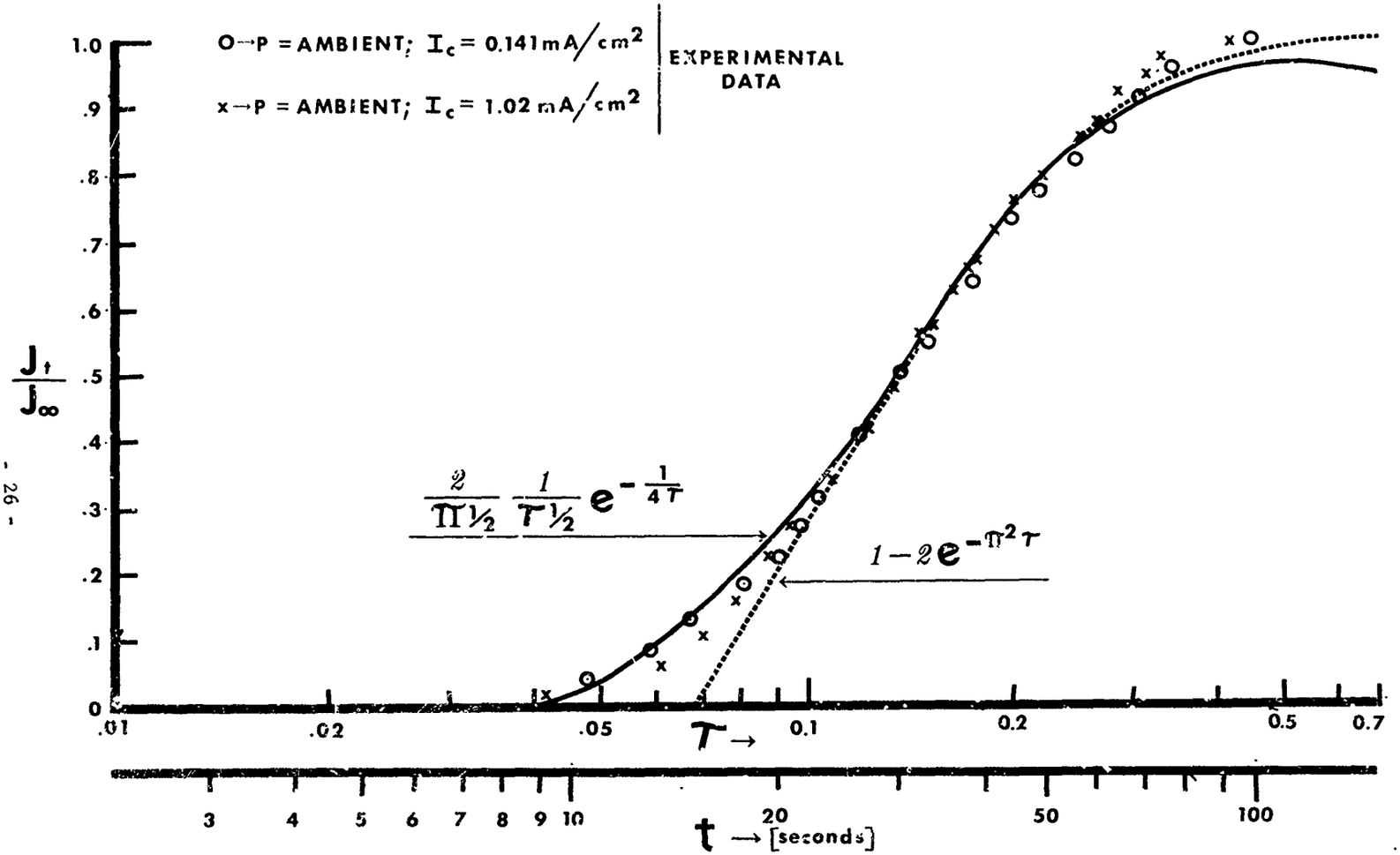

FIG. 6 COMPARISON OF EXPERIMENTAL DATA WITH THEORETICALLY PREDICTED TRANSIENTS AT AMBIENT PRESSURE

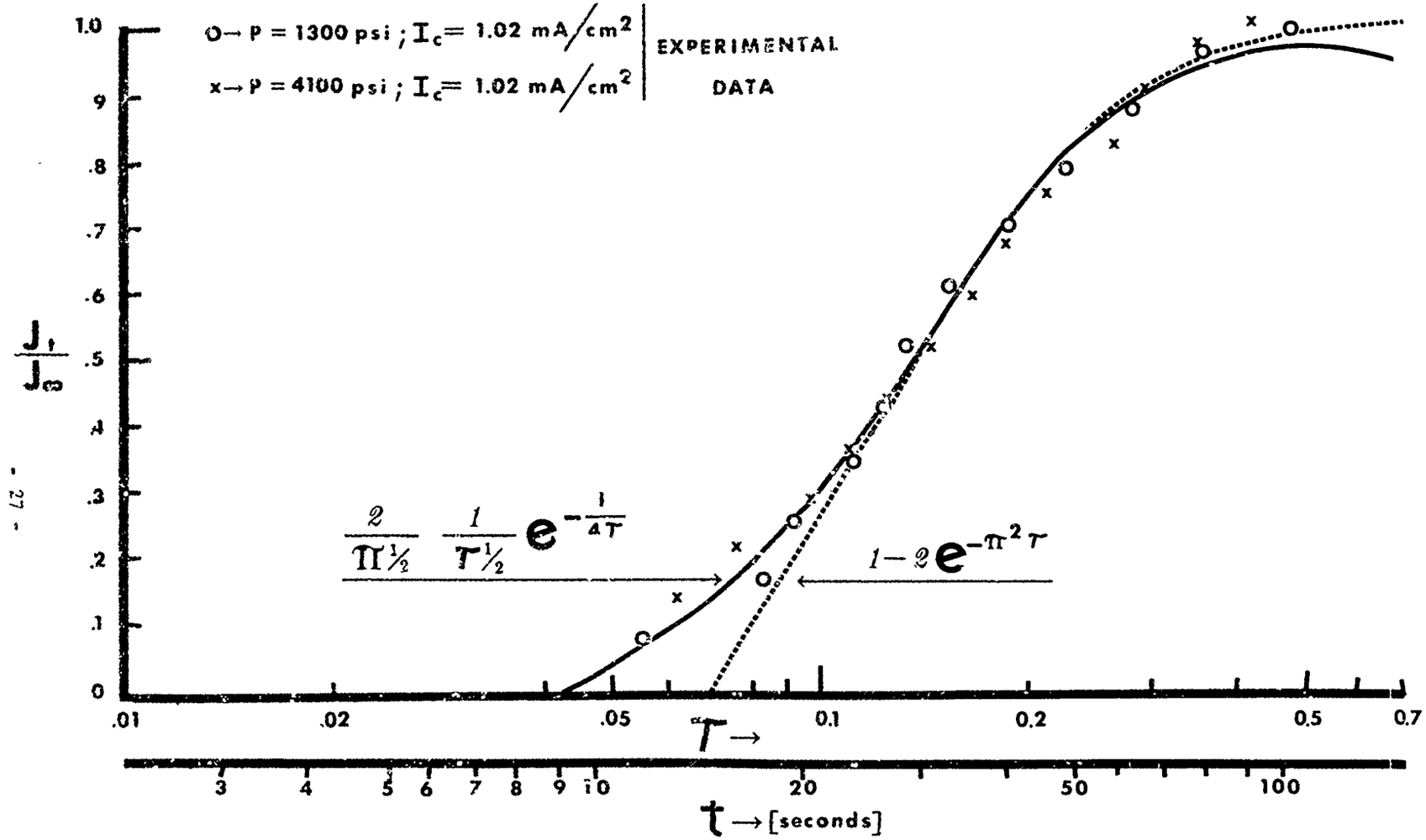

FIG. 7 COMPARISON OF EXPERIMENTAL DATA AT HIGH PRESSURES WITH THEORETICALLY PREDICTED TRANSIENTS

NADC-MA-6726

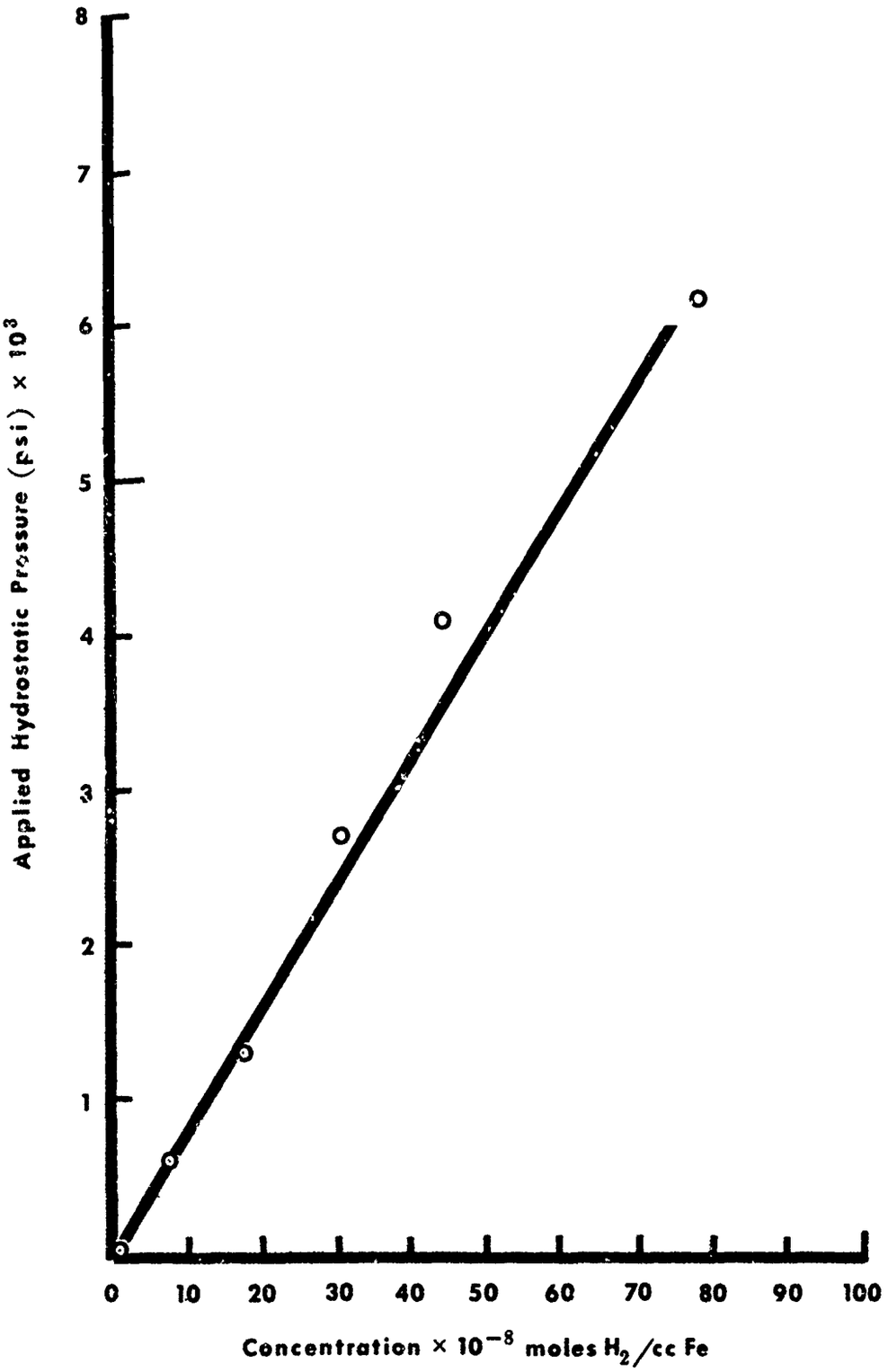

FIG. 8 CONCENTRATION H_2 vs. APPLIED PRESSURE AT 21°C

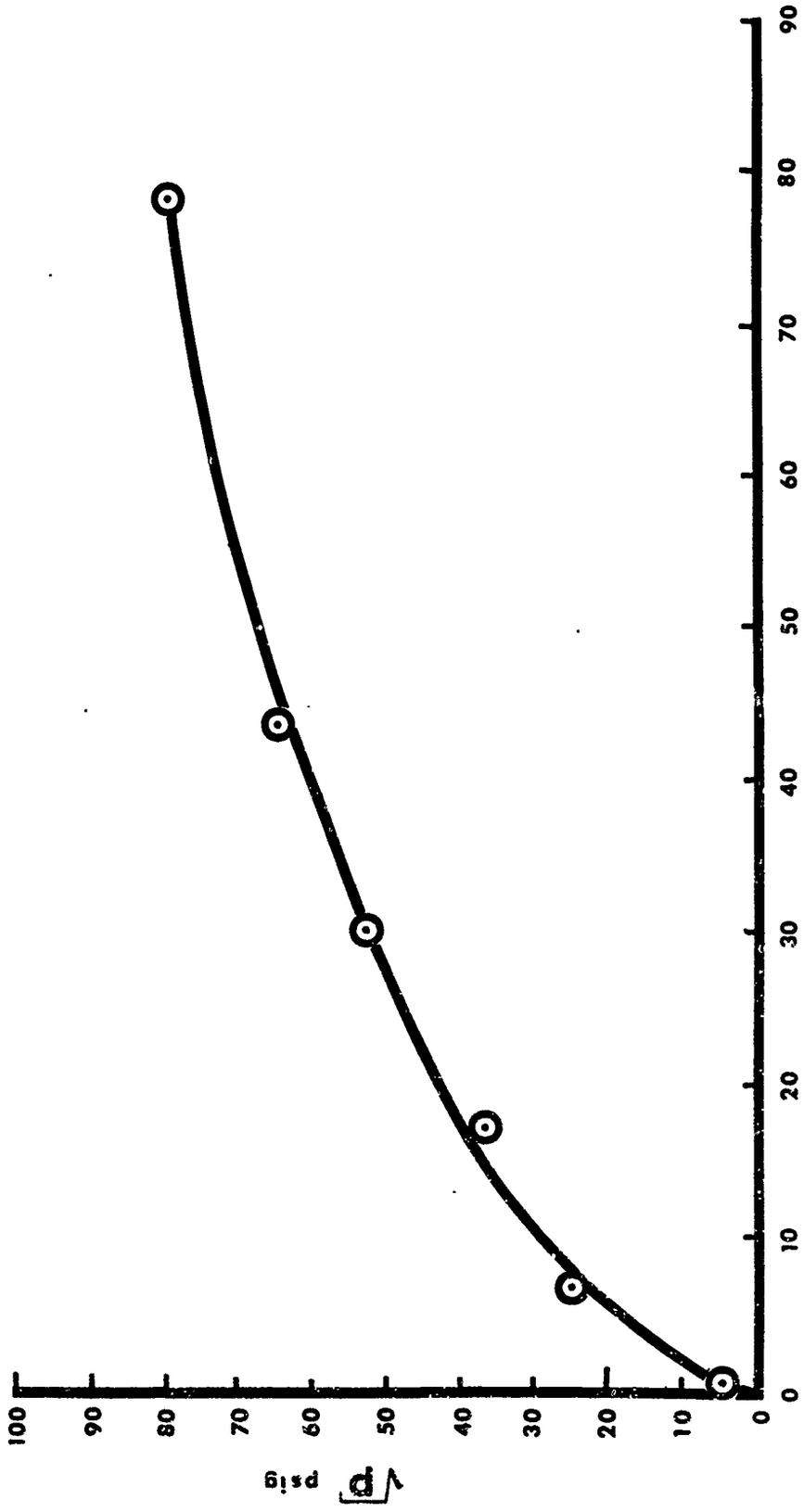

FIG. 9 CONCENTRATION OF HYDROGEN vs. SQUARE ROOT OF PRESSURE AT 21°C

TABLE 3

PRESSURE PERMEATION DATA, ARMCO IRON, L = 0.96 mm., T = 21°C, 0.1N H_2SO_4 + 0.001N HCl

Pressure psi	D, $cm^2\ sec^{-1}$	C_0 moles H_2/ccFe
Ambient	4.1×10^{-5}	0.3×10^{-8}
1300	4.3×10^{-5}	17×10^{-8}
4100	4.4×10^{-5}	44×10^{-8}
6200	4.2×10^{-5}	78×10^{-8}

3. Effect of Pressure on Hydrogen Overpotential

The activation overpotential η, was plotted as a function of the imposed cathodic current density at various pressures and is shown in Figure 10. The experimental points were fitted with a curve based on the values; $\alpha = 0.44$ and I_0 (exchange current density) = 0.08 mA/cm^2. The theoretical curve was obtained from machine computed tables, reference (m), for α, the symmetry factor; and the two exponential terms of the following rate equation:

$$I = I_0 \left[\exp\left(\frac{\alpha ZnF}{RT}\right) - \exp\left(-\frac{(1-\alpha)ZnF}{RT}\right) \right] \qquad (41)$$

where the absolute value of η is used.

The relationship between the steady state permeation current density and the imposed cathodic current density at ambient pressure is shown in Figure 11 where the square of the permeation current is plotted against the cathodic current on the basis of a possible mechanism scheme to be discussed in Discussion, paragraph 3. It should be noted that a good fit of this data may also be obtained with a plot of permeation current density versus the 3/2 power of cathodic current as shown in Figure 12. The 3/2 exponent is chosen semi-empirically since many hydrogen evolution reaction schemes lead to predicted exponents in the same range. It should be also noted, however, that these exponents are usually derived (c.f. Table 1) on the basis of Tafel behavior in the relationship between current density and overpotential. The present results are in a region of the I - η relation which is in transition from linear to Tafel behavior.

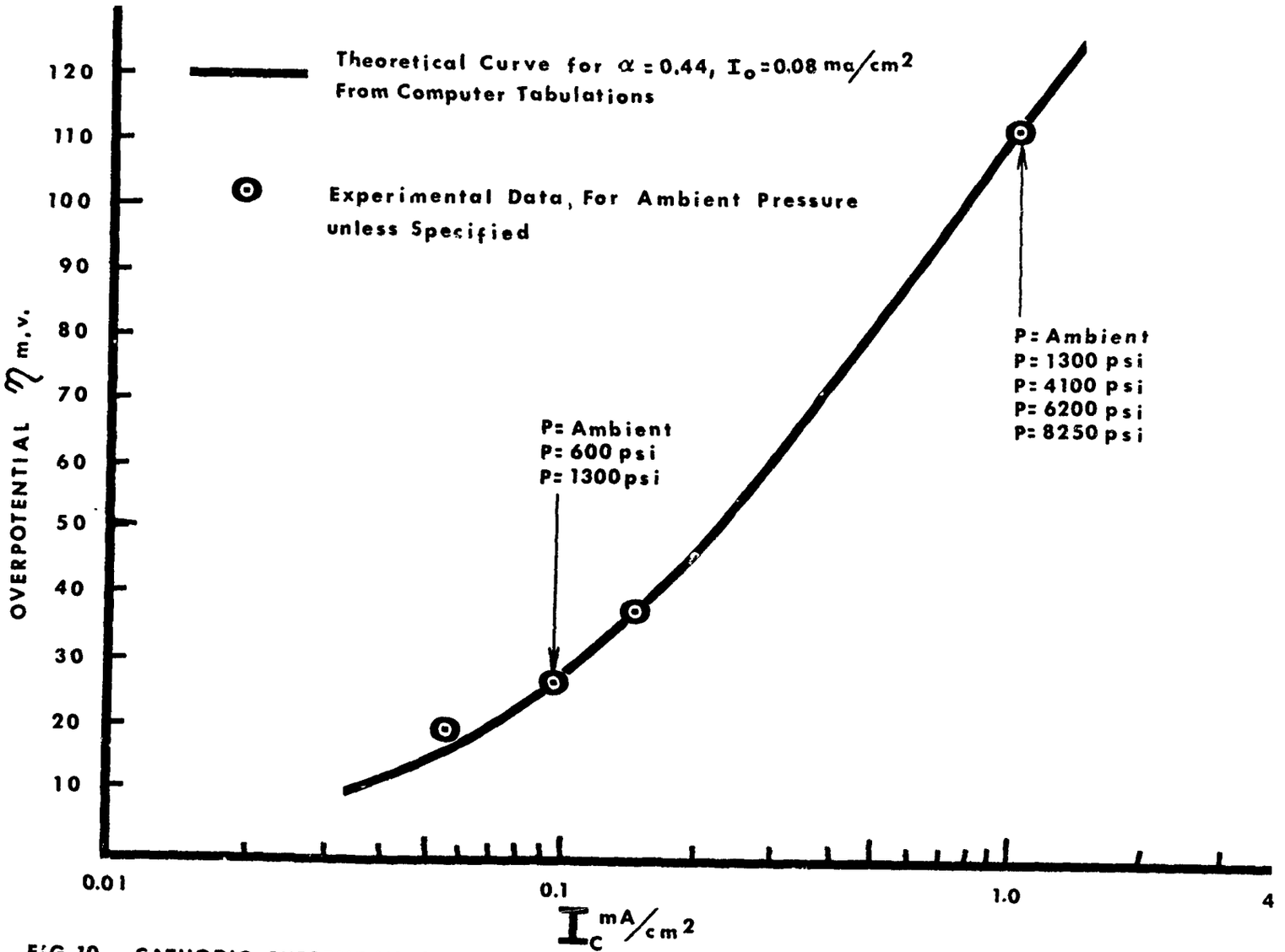

FIG. 10 CATHODIC CURRENT VS. OVERPOTENTIAL FOR ARMCO IRON IN 0.1N H_2SO_4 + .001N HCl

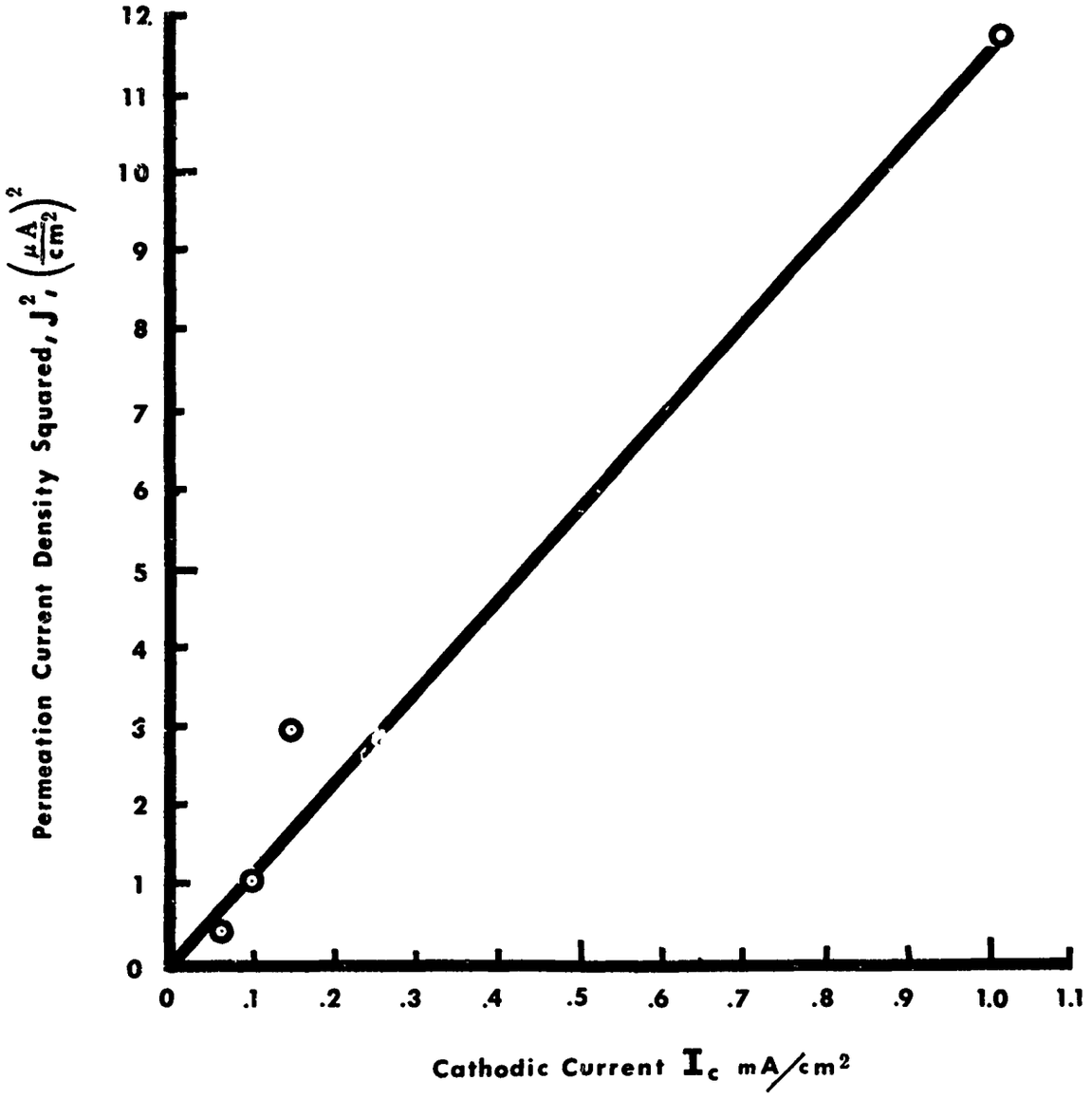

FIG.11 STEADY STATE PERMEATION CURRENT SQUARED VS. IMPOSED CATHODIC CURRENT

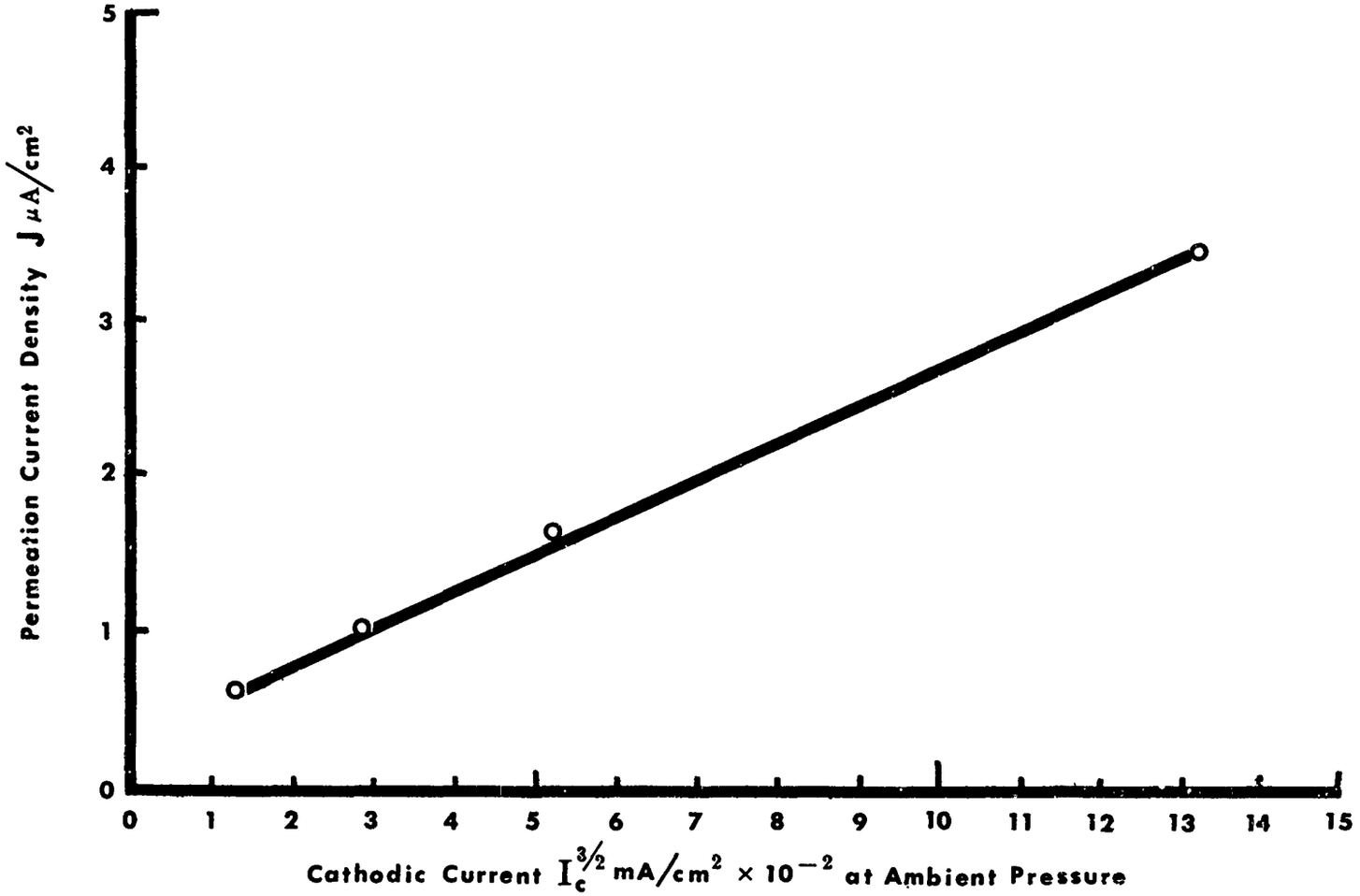

FIG.12 STEADY STATE PERMEATION CURRENT vs. SQUARE ROOT OF CATHODIC CURRENT CUBED

D I S C U S S I O N

1. Pressure Effects on Residual Hydrogen Permeation

In Figure 5, it may be seen that pressure appears to increase the residual permeation current in a linear fashion up to about 5000 psi. Between 6000 and 8000 psi, a marked increase in the residual current is noted. The increase in the residual permeation curve clearly indicates an increase in hydrogen solubility at the input surface. The applied pressure on the cathodic compartment is essentially the partial pressure of hydrogen above the solution. According to the Langmuir (and other) adsorption isotherm, the higher hydrogen partial pressure tends to produce more adsorbed atomic hydrogen on the surface, i.e. θ increases. The increased solubility is manifested by an increased permeation residual since more current is needed to maintain the requirement of zero hydrogen concentration at the anodic (potentiostated) side. The twelve seconds in which a steady state residual current is established during a pressure change is most probably due to the fact that this amount of time is required by the pressure pump to achieve the desired pressure and is not due to an increase in time imposed by the increased hydrogen solubility at the surface. Since this effect is reversible, no permanent lattice distortion is believed to occur. Such phenomena as the marked increase in the residual current above a pressure of 6000 psi might be expected if on reaching a critical hydrogen concentration in the metal, precipitation of a surface metal hydride occurs and grows progressively into the metal with time. It is recalled that establishment of a steady state residual permeation current required 19 minutes at the 8250 psi level. This time interval may be associated with nucleation and growth process of a metal hydride phase. The increase in the permeation rate may be caused by the hydride having a higher diffusion coefficient for hydrogen than the iron. Since metal hydrides are known to be unstable, removal of the pressure could be expected to restore the original permeation properties to the iron as was experimentally observed, i.e. phenomenon reversibility. It should be noted that all previous elevated pressure hydrogen studies, references (n) and (o), on iron were also performed at elevated temperatures and as such, a pressure induced hydride phase would be negated by the temperature instability of such a phase.

2. Pressure Effects on the Diffusion Coefficient and Solubilities of Hydrogen in Alpha Iron

The diffusion coefficient at ambient pressure was found to be 4.3×10^{-5} cm^2 sec^{-1} as opposed to 6.25×10^{-5} cm^2 sec^{-1} found by McBreen, et.al., reference (p), using the same technique. This slight disparity may be due to the lower temperature (21°C vs. 25°C) and coarser grain structure of the iron (ASTM #7 vs. #10) for the present work. The lower temperature and the decreased grain boundary area will cause a decrease in the diffusion

rate. The effect of pressure to 6000 psi on the diffusion coefficient appears to be negligible (c.f. Table 3, Figures 6 and 7). This is not surprising since these pressures will cause negligible lattice distortion even in the elastic range. The solubility of hydrogen as shown by C_0 in Table 2 is seen to increase with applied pressure. A plot of hydrogen concentration against applied pressure (c.f. Figure 8) exhibits a linear relationship. A deviation from linearity most probably occurs above 6000 psi because of the marked increase in permeation above this pressure. Figure 9 exhibits a positive deviation from the well-known Sieverts' relationship of linear solubility with the square root of pressure; the exponent of the pressure is greater than 1/2 and is, in fact, unity. The positive deviation from Sieverts' behavior is in agreement with the work of Johnson and Hill, reference (n), who used vacuum and thermal extraction techniques to study H_2 in iron and found positive deviations from the Sieverts' pressure exponent of 1/2 at "low" temperatures, the lowest being 145°C. The solubility calculated from the data of Johnson and Hill, reference (n), for H_2 in iron at 1470 psi (gaseous) and 145°C is 23 times as large as that of this work at 21°C at the same pressure. The diffusion coefficient for H_2 in iron calculated by Johnson and Hill in an earlier work, reference (o), is $D_{25°C} = 2.2 \times 10^{-5}$ cm^2 sec^{-1}. Since the experimental data of Johnson and Hill rely on a vacuum extraction transient, the agreement between their result and the present value of $D_{21°C} = 4.3 \times 10^{-5}$ cm^2 sec^{-1} must be considered quite good. Geller and Sun, reference (q), in a study of hydrogen diffusion in iron indicate that the solubility of hydrogen in iron at room temperature and atmospheric pressure should be less than 0.005 cc. H_2/100g Fe (3.49×10^{-8} moles H_2/cc. Fe), which is in accord with the calculated ambient pressure solubility of this work (c.f. Table 3). The Geller-Sun diffusion coefficient is $D_{25°C} = 1.6 \times 10^{-5}$ cm^2 sec^{-1}.

It is again emphasized that the effect of grain size on the diffusion coefficient of hydrogen in iron is most probably important. Early workers used methods which were not sensitive enough to detect the effect of grain boundaries on D. A systematic study of the effect of grain size on the diffusion of hydrogen in iron is needed.

3. Pressure Effect on Hydrogen Overpotential

The computer tabulated fit of the experimental activation overpotential (c.f. Figure 10) yields a symmetry factor $\alpha = 0.44$ and an exchange current density, $I_0 = 0.08$ mA/cm^2. From Figure 10, it is noted that the overpotential-current range is in transition from linear to Tafel behavior, that is, true Tafel behavior begins at some current density in excess of 0.2 mA/cm^2. Since only one current density is experimentally available in the Tafel region (e.g. 1.02 mA/cm^2), estimation of the Tafel slope by the traditional graphical method has not been used but is based on the fitted value of $\alpha = 0.44$ yielding

$$\frac{\partial \eta}{\partial \ln I_c} = 0.138 \text{ V/decade of current density} \qquad (42)$$

It should be emphasized that the rate equations for reactions (Equations (4), (5), and (6)) listed in Background, paragraph 2, and used to develop the relationships of Table 1 are only valid within the Tafel region of the current-potential relationship. Since only low cathodic current densities were chosen for this study (in order to avoid the irreversible critical amount of hydrogen phenomenon encountered by McBreen (reference (p)), the experimentally defined regime of Figure 10 is predominantly linear and as such is not governed by the exponential rate equations. The rate equations for reactions (Equations) (4), (5), and (6) that govern kinetic behavior in the linear region are as follows where exponential terms have been expanded and second order and higher terms have been dropped:

$$I_4 = FK_4 \ (1-\theta)a_{H_3O^+} \left[1 - \frac{\alpha F\eta}{RT}\right] \ ; \ I_{-4} = FK_{-4}\,\theta \left[1 + \frac{(1-\alpha)\,F\eta}{RT}\right] \qquad (43)$$

$$I_5 = K_5(\theta)^2 \ ; \ I_{-5} = K_{-5}\,(1-\theta)^2\,pH_2 \qquad (44)$$

$$I_6 = FK_6\,\theta\,a_{H_3O^+} \left[1 - \frac{\alpha F\eta}{RT}\right] \ , \ I_{-6} = FK_{-6}(1-\theta)p_{H_2} \left[1 + \frac{(1-\alpha)\,F\eta}{RT}\right] \qquad (45)$$

Within the linear region, the rates of electron exchange with oxidized and reduced species are comparable so that the reverse direction rate equations cannot be ignored. If the discharge reaction, Equation (4), proceeds at a rate which is much more rapid than the succeeding step, we may write:

$$FK_4\,(1-\theta)a_{H_3O^+} \left[1 - \frac{\alpha F\eta}{RT}\right] = FK_{-4}\,\theta \left[1 + \frac{(1-\alpha)\,F\eta}{RT}\right] \qquad (46)$$

The Langmuir relationship extracted from Equation (46) is,

$$\frac{\theta}{(1-\theta)} = \frac{K_4\,a_{H_3O^+}\left[1 - \frac{\alpha F\eta}{RT}\right]}{K_{-4}\left[1 + \frac{(1-\alpha)\,F\eta}{RT}\right]} \qquad (47)$$

Since a net flux (current) for reaction (5) is the difference in the forward and reverse reaction rates, we have,

$$I_{net} = FK_6 \; \theta \; a_{H_3O^+} \left[1 + \frac{\alpha Fn}{RT}\right] - FK_{-6} (1-\theta) p_{H_2} \left[1 + \frac{(1-\alpha) Fn}{RT}\right] \qquad (48)$$

For $\theta \ll 1$, Equation (47) becomes,

$$\theta = \frac{K_4}{K_{-4}} \frac{a_{H_3O^+} \left[1 - \frac{\alpha Fn}{RT}\right]}{\left[1 + \frac{(1-\alpha) Fn}{RT}\right]} \qquad (49)$$

Substitution of Equation (49) in Equation (48) yields an extremely complex relationship that does not permit a simple evaluation of parameters as may be done in the Tafel region nor can predictions of the pressure dependence of the overpotential be readily made. However, for high coverage conditions, i.e. $\theta \simeq 1$, Equation (48) becomes

$$I_{net} = FK_6 \; a_{H_3O^+} \left[1 - \frac{\alpha Fn}{RT}\right] \qquad (50)$$

so that

$$\frac{\partial n}{\partial I} = - \frac{RT}{K' \alpha F} \qquad (51)$$

where $K' = FK_6 \; a_{H_3O^+}$

Equation (50) also satisfies the required pressure independence of the overpotential since the second term of Equation (48) is negligible. Assuming a net current for the catalytic combination reaction, Equation (5), we have

$$I_{5_{net}} = FK_5(\theta)^2 - FK_{-5}(1-\theta)^2 \; p_{H_2} \qquad (52)$$

Where $\theta \ll 1$, the insertion of the Langmuir equation in terms of overpotential (Equation (47)) does not yield the required pressure independence. When $\theta \simeq 1$, the second term of Equation (52) drops out yielding

$$I_{5_{net}} = FK_5 \theta^2 \qquad (53)$$

It should be noted that Figure 11, exhibits linearity in a plot of cathodic current density vs. square of permeation current, which would be consistent with the first term of Equation (52) indicating that fast discharge in combination with slow catalytic combination, for large hydrogen coverage ($\theta \simeq 1$), must be considered as a possibility for the reaction sequence of the hydrogen evolution reaction under the present conditions. To complete the picture, it should be stated that a choice between sequential Equations (4) - (5) and Equations (4) - (6) cannot be made entirely on the basis of the present data. If Equation (50) is returned to exponential form (Tafel), the slope is in agreement with the slope predicted on the basis of full Tafel behavior, listed in Table 1 (c.f. Equation (42)). This would tend to confirm sequence Equations (4) - (6) while equally strong evidence based on Equation (53) and shown in Figure 11 lends support to sequence Equations (4) - (5). Both conjectured sequences provide pressure independence for the overpotential at high hydrogen coverage. Further work both theoretical and experimental is needed to exploit this relatively untouched area (linear I - n) for diagnosis of electrode kinetics.

4. Phenomenology Established

The following room temperature phenomena were established during the course of this work:

a. Applied hydrostatic pressure increases the residual hydrogen permeation rate in iron in a linear fashion to abo' 6000 psi. A marked increase in the permeation rate occurs between 600c and 8000 psi possibly indicating the existence of an unstable hydride phase.

b. The pressure effects on permeation are reversible within the range from 0 to 8,250 ps applied pressure.

c. Hydrostatic pressures to 6200 psi do not affect the diffusion coefficient of hydrogen in Armco iron.

d. Solubility of hydrogen in Armco iron is proportional to the applied hydrostatic pressure (viz. hydrogen partial pressure) at least up to 6000 psi at 21°C; indicating a positive deviation from Sieverts' square root of pressure relationship.

e. The partial pressure of hydrogen (i.e. applied hydrostatic pressure) does not affect the hydrogen overpotential on iron in 0.1N H_2SO_4 + 0.001N HCl.

The increased solubility of hydrogen in iron at elevated pressures and low temperatures (21°C) uncovered in this work, necessitates an increased concern for the role of hydrogen in environmental cracking of alloys destined to be used in the deep ocean environment. Further, the absence of a hydrostatic pressure effect on the diffusion coefficient of hydrogen in iron indicates minimal lattice distortion and is a fact helpful in picturing the migration of H_2 in an elastic stress field.

A C K N O W L E D G E M E N T S

The author owes a large debt of gratitude to Professor Leonard Nanis for his unbounded provision of technical guidance, intellectual stimulation and encouragement during the course of this work.

The author also wishes to thank Mr. J. A. Piland and Mr. E. Taylor for their help and cooperation. A special note of thanks is due Mr. F. Pace whose craftsmanship made many of the intricate designs a reality.

REFERENCES

(a) Troiano, A. R.: Trans ASM, 52, 54 (1960)

(b) Shively, J. H., Hehemann, R. F., and Troiano, A. R.: Corrosion, 22, 9, 253 (1966)

(c) Devanathan, M.A.V. and Stachurski, Z.: Proc. Roy. Soc., A270 (1962)

(d) Richardson, O. W., Nicol, J., and Parnall, T.: Phil. Mag., (6), 8, 1 (1904)

(e) Sieverts, A., Krumbharr, W., and Jurisch, E.: Z. Phys. Chem., 77, 591 (1911)

(f) Borelius, G., and Lindblom, J.: Ann. Physik., (4), 82, 201 (1927)

(g) Heath, H. R.: British J. Appl Phys., 3, 13 (1952)

(h) Frumkin, A. N. and Bagotskaya, I. A.: Doklady. Akad. Nauk., 92, 979 (1953)

(i) Conway, B. E.: Theory and Principles of Electrode Processes, Ronald Press, New York, N. Y., 1965, p. 80

(j) Mc Breen, J., Nanis, L., and Beck, W.: J. Electrochem. Soc., 113, 11, 1218 (1966)

(k) Ives, D. and Janz, G.: Reference Electrodes, Ch. 4, Academic Press (1961)

(l) Gionnoscoli, J.: Private Communication at Aero Materials Department

(m) Nanis, L.: Private Communication

(n) Johnson, E. W. and Hill, M. L.: Trans. AIME, 221, 622, (June 1961)

(o) Johnson, E. W. and Hill, M. L.: Trans. AIME, 118, 1104, (Dec 1960)

(p) McBreen, J., Nanis, L., and Beck, W.: Contract No. N156-44134, Naval Air Engineering Center, Final Report, (14 Nov 1964)

(q) Geller, W. and Sun, Tak-Ho: Archiv fur das Eisenhuttenwesen, 21 Jahrgang, 423 (1950)

B I B L I O G R A P H Y

Baukloh, W. and Retzlaff, W.: Arch. Eisenhutenwesen, 11, 97

Bockris, J. O'M. and Parsons, R.: Trans. Farad Soc., 45, (916) (1949)

Bodenstein, M.: Z. Electrochem., 28, 517 (1922)

Borelius, G. and Lindblom. J.: Ann. Physik, (4), 82, 201 (1927)

Conway, B. E.: Theory and Principles of Electrode Processes, Ronald Press, New York, N. Y. (1965)

Devanathan, M.A.V. and Stachurski, Z.: Proc. Roy. Soc., A270, (1962)

Devanathan, M.A.V.: Chem. Rev., 1965, 65

Edwards, C. A. and Pfiel, I. B.: J. Iron Steel Inst., 110, 123 (1924)

Frumkin, A. N. and Bagotskaya, I. A.: Doklady Akad. Nauk., 92, 979 (1953)

Geller, W. and Sun, T-H.: Archiv fur das Eisenhuttenwesen, 21 Jahrgang (1950)

Heath, H. R.: British J. Appl. Phys., 3, 13 (1952)

Hills, G. J. and Kinniburgh, D. R.: J. Electrochem. Soc., 113, 11 (1966)

Horiuti, J. and Polanyi, M.: Acta Physicochim, 2, 505 (1935)

Ives, D. and Janz, G.: Reference Electrodes, Ac. Press (1961)

Johnson, E. W. and Hill, M. L.: Trans. AIME, 118 (1960)

Johnson, E. W. and Hill, M. L.: Trans. AIME, 221 (1961)

Kita, H.: J. Electrochem. Soc., 113, 11 (1966)

Mathews, D. B.: The Mechanism of Hydrogen Evolution Reaction, Ph.D. Dissertation, University of Pennsylvania (1965)

McBreen, J., Nanis, L., and Beck, W.: J. Electrochem. Soc., 113, 11 (1966)

McBreen, J., Nanis, L., and Beck, W.: Contract No. N156-44134, Naval Air Engineering Center, Final Report (14 Nov 1964)

McBreen, J.: The Permeation of Electrolytic Hydrogen Through Iron, Ph.D. Dissertation, University of Pennsylvania (1965)

Perminov and V'Yunov: Korroziya - USSR, 4 (1938)

Roychoudury and Bonilla: J. Electrochem. Soc., 103 (1956)

Shively, J. H., Hehemann, R. F., and Troiano, A. R.: Corrosion, 22 9 (1966)

Sieverts, A., Krumbharr, W., and Jurisch, E.: Z. Phys. Chem., 77 (1911)

Smialowski, M.: Hydrogen in Steel, Pergamon Press (1962)

Smithells, C. J.: Gases and Metals, John Wiley & Sons, New York (1937)

Tafel, J.: Z. Phys. Chem., 50 (1905)

Troiano, A. R.: Trans. ASM, 52 (1950)

Vetter, K. J.: Electrochemishe Kinetik Springer-Verlag (1961)

Vetter, K. J. and Otto, D.: Z. fur Electrochem., 60 (1956)

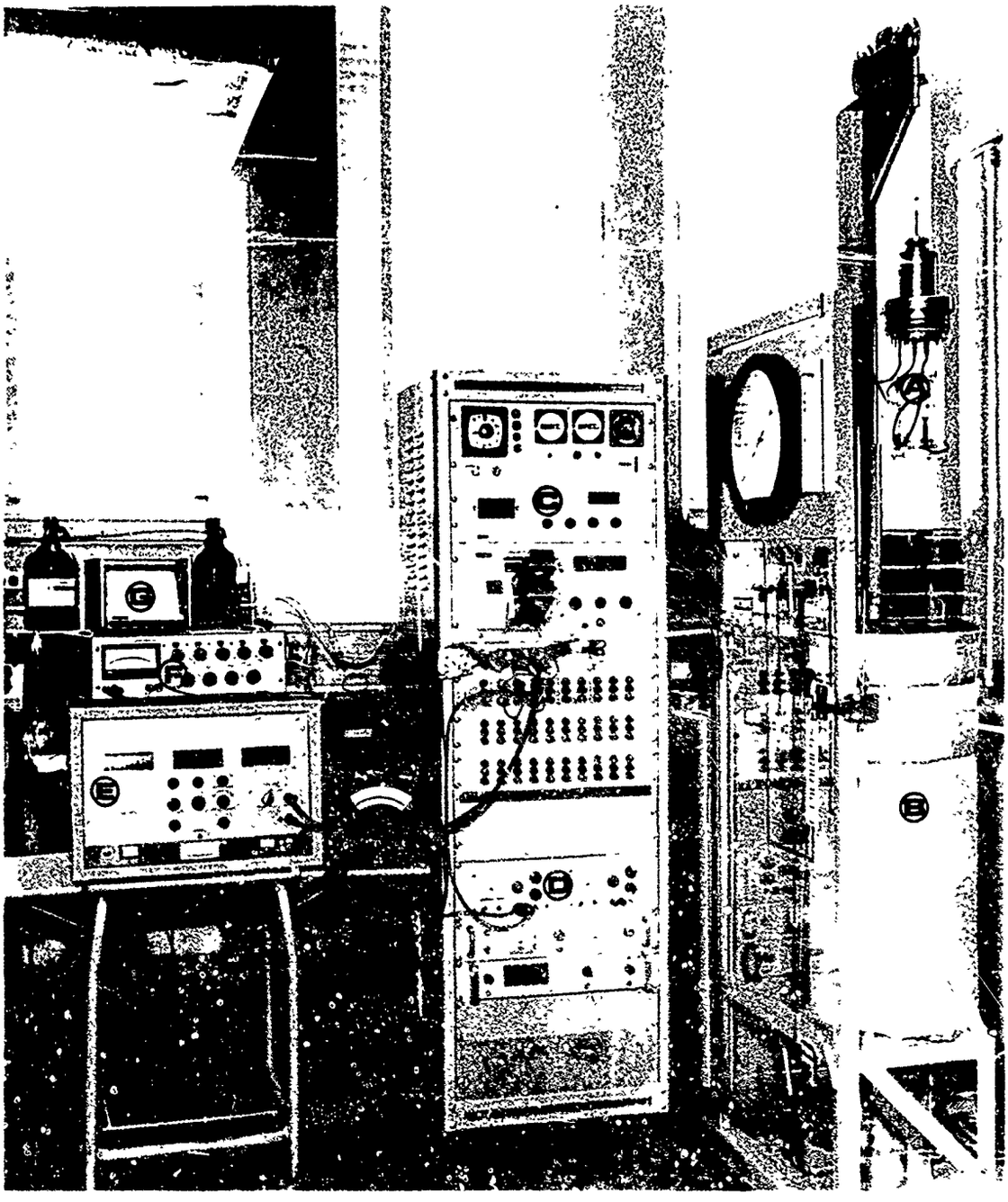

PANORAMA OF THE EXPERIMENT

A. ELECTROCHEMICAL CELL SUSPENDED ABOVE PRESSURE VESSEL
B. ENVIRONMENTAL SIMULATION UNIT
C. DIGITAL VOLTMETER AND PRINTER
D. D.C. POWER SUPPLY
E. ELECTRONIC POTENTIOSTAT
F. AMPLIFYING ELECTROMETER
G. STRIP CHART CURRENT RECORDER

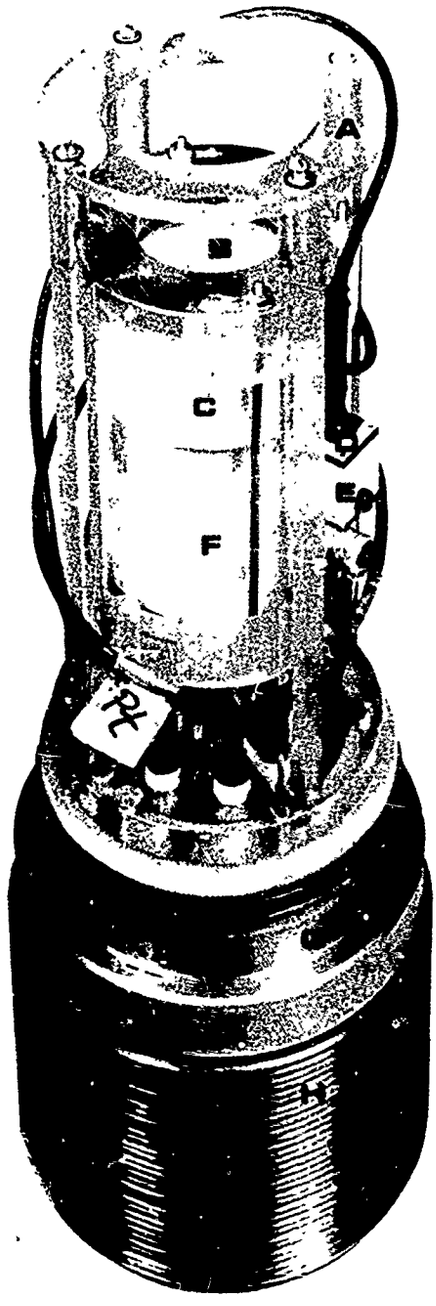

ASSEMBLED ELECTROCHEMICAL CELL

A. PLEXIGLASS FRAME
B. TIMPANIC MEMBRANE
C. CATHODIC COMPARTMENT
D. HIGH PRESSURE ELECTRICAL CONNECTOR
E. SPECIMEN HOLDER
F. ANODIC COMPARTMENT
G. MONEL PRESSURE VESSEL HEAD
H. STEEL RETAINING RING

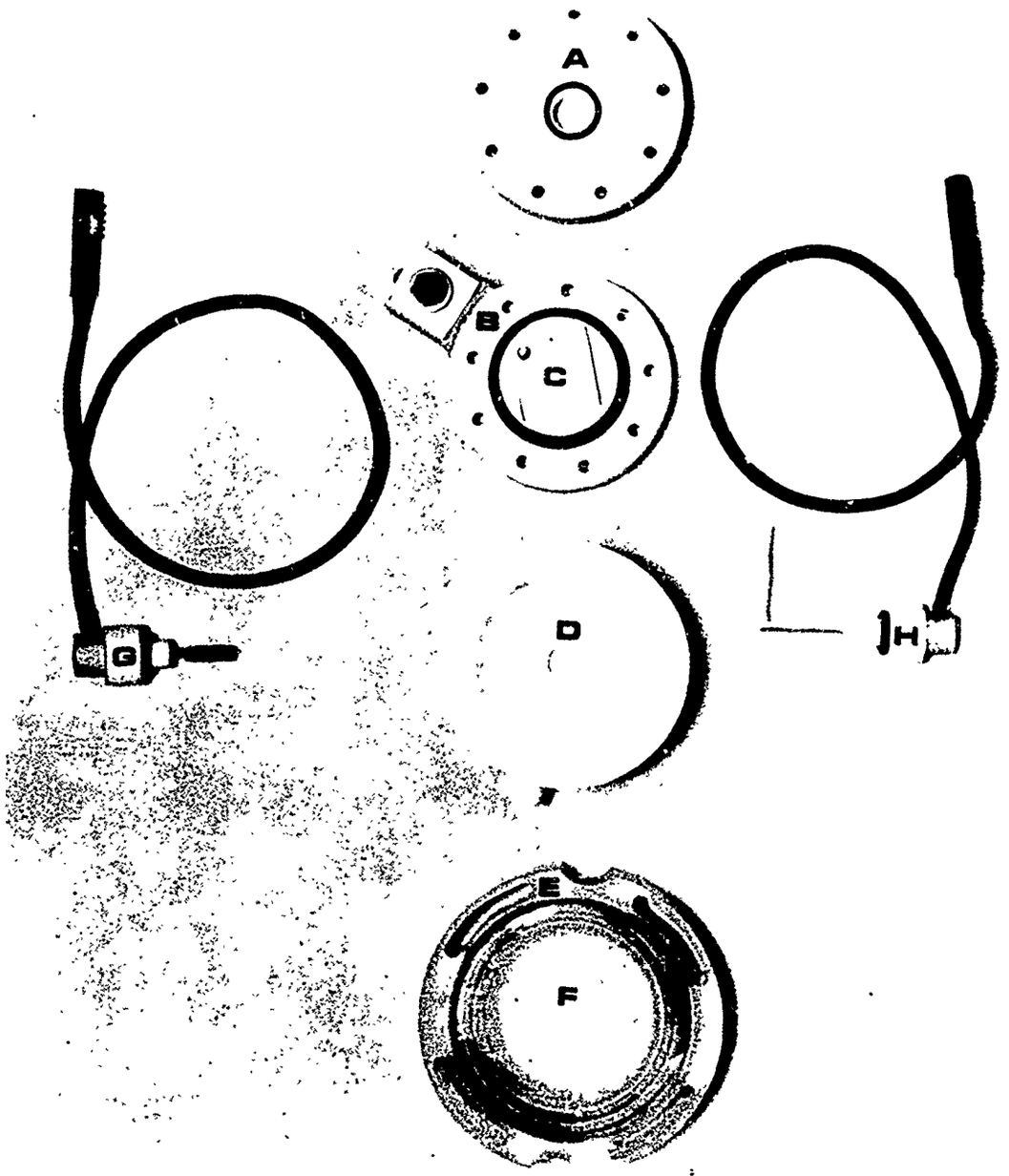

DISASSEMBLED ELECTROCHEMICAL CELL

A. SPECIMEN HOLDER, TOP HALF
B. SPECIMEN HOLDER, BOTTOM HALF
C. METAL SPECIMEN
D. TIMPANIC (CATHODIC OR ANODIC) COMPARTMENT
E. PLEXIGLAS RETAINING RING
F. TIMPANIC MEMBRANE
G. PLATINUM COUNTER ELECTRODE
H. Ay-Agll REFERENCE ELECTRODE (WITH GLASS CAPILLARY)

UNCLASSIFIED

Security Classification

DOCUMENT CONTROL DATA - R & D

(Security classification of title, body of abstract and indexing annotation must be entered when the overall report is classified)

1 ORIGINATING ACTIVITY (Corporate author) AERO MATERIALS DEPARTMENT NAVAL AIR DEVELOPMENT CENTER, JOHNSVILLE WARMINSTER, PA. 18974	2a. REPORT SECURITY CLASSIFICATION UNCLASSIFIED 2b GROUP None

3 REPORT TITLE

THE EFFECTS OF HYDROSTATIC PRESSURES TO 8250 PSI ON ELECTROLYTIC HYDROGEN IN IRON

4 DESCRIPTIVE NOTES (Type of report and, inclusive dates)

5 AUTHOR(S) (First name, middle initial, last name)

JOHN J. DE LUCCIA

6 REPORT DATE	7a. TOTAL NO OF PAGES	7b. NO OF REFS
24 January 1968	47	17

8a. CONTRACT OR GRANT NO	9a. ORIGINATOR'S REPORT NUMBER(S)
b. PROJECT NO	NADC-MA-6726
c IR Task No. R011-01-01 - WU No. 33	9b OTHER REPORT NO(S) (Any other numbers that may be assigned this report)
d	None

10 DISTRIBUTION STATEMENT

This document has been approved for public release and sale; its distribution is unlimited.

11 SUPPLEMENTARY NOTES	12 SPONSORING MILITARY ACTIVITY
None	NAVAL AIR SYSTEMS COMMAND DEPARTMENT OF THE NAVY WASHINGTON, D. C. 20360

13 ABSTRACT

An apparatus for the determination of electrochemical parameters as well as diffusion parameters of hydrogen in iron at hydrostatic pressures up to 20,000 psi using the hydrogen permeation technique is described. Values of the diffusion coefficient and solubility of hydrogen in iron at pressures to 8250 psig are listed. The effect of pressure on the cathodic hydrogen evolution kinetics is noted. All experiments were performed on Armco iron in 0.1N H_2SO_4 + 0.001N HCl at 21°C.

DD FORM 1 NOV 65 1473 (PAGE 1)

S/N 0101-807-6811

UNCLASSIFIED

Security Classification

A-31408

14 KEY WORDS	LINK A		LINK B		LINK C	
	ROLE	WT	ROLE	WT	ROLE	WT
Hydrogen Evolution Kinetics						
Diffusion Coefficient						
Timpanic Permeation Cell						
Reference Electrodes						
Electrochemical H_2 Permeation						
Environmental Cracking						
Hydrostatic Pressure						
Pressure Vessel						

END